

Internal tides modelling in the Bay of Biscay. Comparisons with observations

ANNICK PICHON¹ and STEPHANIE CORREARD²

¹ Service Hydrographique et Océanographique de la Marine, Centre Militaire d'Océanographie, 13 rue le Chatellier
B.P. 30316, 29603 Brest Cedex, France. E-mail pichon@shom.fr

² Société HOCER, 5 rue Eugène Bourdon ZI de Kergaradec, 29490 Guipavas, France.

SUMMARY: An Isopycnic Coordinate Ocean Model is used to represent the three-dimensional propagation of internal tides in the Bay of Biscay. The model is forced by the semi-diurnal tidal waves M2, S2, N2 and K2. A high resolution topography of French and Iberian continental slopes preserves the shape of the main canyons, which are areas of internal tide generation. Hydrological and velocity data collected during a French Naval experiment in 1994 are compared with the model results. Near the generation area, the vertical distribution of the internal tide amplitude, associated with a vertical shear of baroclinic tidal currents, is in agreement with the observations. Moreover, at most locations, the increase in the baroclinic current modelled near the bottom depth matches the data. This increase is related to the distribution of the internal tide amplitude along the ray slope defined by

$$c(z) = \left(\frac{w^2 - f^2}{N^2(z)} \right)^{1/2},$$

where w is the tidal frequency, f the Coriolis parameter and $N(z)$ the buoyancy frequency. In most of the data/model comparisons, the vertical density variation in the deep layers shows a difference in phase in agreement with the ray theory. Over the abyssal plain, high horizontal shears of surface current are modelled at mid-bay, i.e. in areas where the internal wave energy coming from the deep ocean encounters the seasonal thermocline. However, the location of these areas is very sensitive to the initial vertical density profile: the three-dimensional variation of the density must be introduced in the initial conditions to improve the model results.

Keywords: internal tide, shelf edge, isopycnal model, observations.

RESUMEN: MODELADO DE LAS ONDAS INTERNAS EN EL GOLFO DE VIZAYA. COMPARACIÓN CON OBSERVACIONES. – Se ha utilizado un modelo de coordenadas isopycnicas para representar la propagación tridimensional de las ondas internas de marea en el Golfo de Vizcaya. El modelo se fuerza por las cuatro ondas de marea semidiurnas M2, S2, N2, K2. Una topografía de alta resolución de los taludes continentales francés y español reproduce la forma de los principales cañones, que son zonas de generación de las ondas internas. Los resultados del modelo se compararon con datos hidrológicos y de corrientes obtenidos en 1994, durante una campaña del Servicio Hidrográfico y Oceanográfico de la Marina francesa. Cerca de la zona de generación, la distribución vertical de la amplitud de la onda interna, asociada a un cizallamiento vertical de las corrientes de marea baroclinas, concuerda con las observaciones. Además, el aumento de intensidad de la corriente baroclinica modelizada cerca del fondo, coincide con los datos en la mayoría de los lugares. Este incremento está ligado a la repartición de la amplitud de la marea interna a lo largo de la pendiente de los rayos definida por

$$c(z) = \left(\frac{w^2 - f^2}{N^2(z)} \right)^{1/2},$$

donde w es la frecuencia de marea, f el parámetro de Coriolis y $N(z)$ la frecuencia de Brunt-Väisälä. En la mayor parte de las comparaciones datos/modelo, la variación vertical de la densidad en las capas profundas muestra una diferencia de fase en concordancia con la teoría de rayos. Sobre la planicie abisal, se han modelado intensas cizallas horizontales de la corriente superficial en el centro del Golfo de Vizcaya, es decir, en áreas donde la energía de la onda interna proveniente del océano profundo se encuentra con la termoclina estacional. Sin embargo, la localización de estas áreas es muy sensible al perfil inicial de densidad: la variación tridimensional de la densidad ha de ser introducida en las condiciones iniciales para mejorar los resultados del modelo.

Palabras clave: ondas internas, talud continental, modelo isopycnal, observaciones.

INTRODUCTION

In a stratified fluid, internal tides are generated by the passage of the astronomical tide above a steep bathymetry variation (e.g. the shelf break). The Bay of Biscay is an area where the internal tides are the most energetic (Baines, 1982). Therefore, their effects in this region have an influence on the circulation over the continental shelf and over the abyssal plain, with an effect on the biological processes. In Pingree *et al.* (1981, 1986) and in the ONDINE85 SHOM (Service Hydrographique et Océanographique de la Marine) experiment, biological and physical observations show that the biomass maximum (zooplankton and phytoplankton) is related to the cooling of the sea surface, where the internal tide amplitude is maximum. Following the theoretical model of Mazé (1987), a two-dimensional model of the Bay of Biscay with a two-layer seasonal thermocline (Serpette *et al.*, 1989; Le Tareau *et al.*, 1993) identifies the presence of cold water areas just above the shelf break as a result of interactions between large amplitude internal tides and mixing processes.

However, the internal tide influence is not restricted to the near-surface layers over the continental shelf. New (1988) uses the linear model of Prinsenberg and Rattray (1975) along a realistic cross-section over the continental slope and the abyssal plain of the Bay of Biscay to model the propagation of the internal tides in the vertical plane. From observations, Pingree and New (1989, 1991) show that the main part of the internal wave energy follows the characteristic ray slope, as was theoretically shown by Prinsenberg and Rattray (1975) and Baines (1982). Other measurements (Pichon and Mazé, 1992) confirm the presence of large amplitude internal tides over the continental slope. Moreover, vertical velocity shears associated with the propagation of solitary internal waves are observed at mid-bay (New and Pingree, 1990), and probably have an effect on the biological process through the mixing process. These previous studies show that there is a horizontal propagation of internal tides coming from many generation areas in the whole bay. Even far away from the shelf break, the circulation is modified by the internal tide propagation on the vertical plane. Therefore, the three-dimensional effects of the topography and the spatial variation of the tidal forcing must be taken into account in order to model the internal tide over the whole Bay of Biscay. Previous realistic studies of

internal tides are developed in other regions, using cross-section models (Craig, 1988; Sherwin and Taylor, 1990; Holloway, 1996; Robertson 2001) and using fully three-dimensional models (Cummins and Oey, 1997; Xing and Davies, 1998a; Holloway, 2001). In this paper, the nonlinear three-dimensional propagation of internal tides in the Bay of Biscay is modelled with the Miami Isopycnic Coordinate Ocean Model (MICOM) developed by Bleck and Smith (1990). The three-dimensionality of this region is an important feature for a good representation of the evolution of internal tides: the chaotic distribution of the topography (many canyons and particular topographic perturbations such as the Meriadzeck Terrace are typical of the French continental slope) and the presence of the French and Spanish shelf breaks further the generation of several directions of internal wave propagation which interfere. The model is forced by the semi-diurnal tidal waves with a realistic topography and stratification. The purpose is to model the effect of the internal tide propagation. Air-sea fluxes and the mixing due to internal tide are not introduced. The results are compared with data collected in the deep ocean during the MINT94 SHOM experiment.

The first part of the paper presents the MINT94 experiment data and the model. In the second part, the modelled barotropic tide is validated and the three-dimensional evolution of the baroclinic tide is described by focusing on the vertical sections where the data were collected. These comments support the comparisons between the modelled and the measured physical parameters that are made in the third part.

MATERIAL AND METHODS

The MINT94 experiment

The purpose of the MINT94 experiment was to achieve a description of the internal tide propagation over the abyssal plain. Measurements were collected along vertical sections perpendicular to the continental slope in order to observe a signature of these waves, mainly generated over the French shelf break. A second objective was to confirm that the Spanish continental slope was a generation area (this feature was modelled in a previous study in which the domain of the Le Tareau and Mazé model (1993) was extended up to Ortelgal Cape).

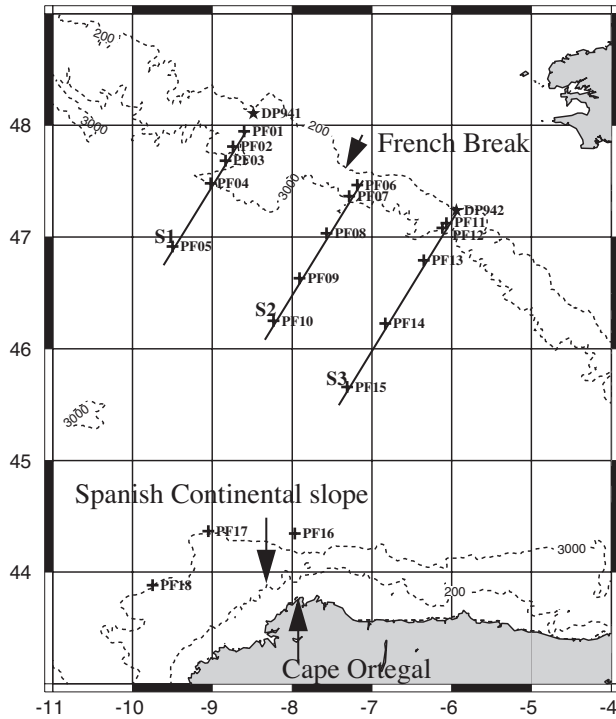


FIG. 1. – Map of the Bay of Biscay showing locations of stations (PF01 to PF18) and moorings (DP94-1 and DP94-2) during the MINT94 experiment (see Table 1 for the experiment details). S1, S2 and S3 are model sections along measurement locations.

Velocity data were collected near the shelf break to evaluate the barotropic forcing term defining the internal tide amplitude in the generation area. In spring 1994, self-contained ADCP, moored on the

bottom at 300 m depth, were deployed at two locations: the DP94-1 and the DP94-2 moorings (Fig. 1). The measurements were recorded for one month in weak stratification conditions. Data processing was performed to extract the depth-averaged velocity (Perenne and Pichon, 1999).

In Autumn 1994, density and velocity data were collected during the first days of September and October, i.e. around the spring tide. At some locations, an ADCP was lowered from the ship with a CTD: hourly “yoyo” stations followed the evolution of the hydrological and velocity parameters over two tidal cycles (25 hours). At other locations, the density was measured by XCTD or XBT launched every half hour. In order to include the deep ocean stratification whilst preserving a sampling frequency of one hour, stations over the abyssal plain were sampled to 2500 m in depth. The French continental slope, the abyssal plain and the Iberian continental slope were sampled. The locations of the stations are plotted in Figure 1. Details of the measurements (position, period, instrument) are summarised in Table 1.

The model

The MICOM equations (Bleck and Smith, 1990) describe rotating, stratified and viscous fluid motions in isopycnic coordinates: the momentum

TABLE 1. – Summary of stations and ADCP moorings during the MINT94 experiment.

Location	Measurement type	Date of measurement (d m h.min)*	Bottom depth (m)	Max station depth (m)	Tidal state (d)**
Station					
PF01	CTD, LADCP	02 Sep 06.19 - 03 Sep 06.08	1500	1500	ST-06
PF02	CTD, LADCP	03 Sep 10.25 - 04 Sep 10.24	2460	2300	ST-05
PF03	XCTD	07 Sep 22.58 - 08 Sep 00.07	3700	2000	ST
PF04	CTD, LADCP	05 Sep 06.05 - 06 Sep 06.22	2850	2300	ST- 03
PF05	XCTD	05 Sep 04.02 - 06 Sep 05.10	4100	2000	ST- 03
PF06	CTD, LADCP	06 Sep 22.36 - 07 Sep 21.38	1100	900	ST- 01
PF07	XBT	11 Sep 02.30 - 12 Sep 02.50	2800	2200	ST+03
PF08	CTD, LADCP	09 Sep 17.00 - 09 Sep 23.50	4350	2500	ST+02
PF09	XCTD	09 Sep 17.30 - 10 Sep 18.30	4800	2000	ST+02
PF10	XCTD	10 Sep 22.05 - 11 Sep 23.05	3950	2000	ST+03
PF11	XCTD	02 Sep 21.00 - 03 Sep 22.09	2100	2000	ST- 05
PF12	CTD	10 Oct 16.30 - 11 Oct 17.08	2700	2230	ST+04
PF13	CTD	09 Oct 13.00 - 10 Oct 14.25	4200	2500	ST+03
PF14	XCTD	03 Oct 06.30 - 04 Oct 07.30	4720	2000	ST- 04
PF15	XCTD	04 Oct 11.30 - 05 Oct 12.50	4850	2000	ST- 03
PF16	CTD	04 Oct 18.45 - 05 Oct 19.30	3700	2250	ST- 02
PF17	XCTD	07 Oct 04.05 - 08 Oct 05.00	3600	2000	ST
PF18	CTD	07 Oct 06.40 - 08 Oct 09.20	3300	2500	ST
ADCP mooring					
DP94-1	ADCP	14 Apr 07.20 - 17 May 07.50	300		
DP94-2	ADCP	18 May 15.00 - 17 Jun 10.00	300		

* The times are given in UT.

** The tidal states are referenced in days, in relation to the Brest Spring tide (ST) for each month.

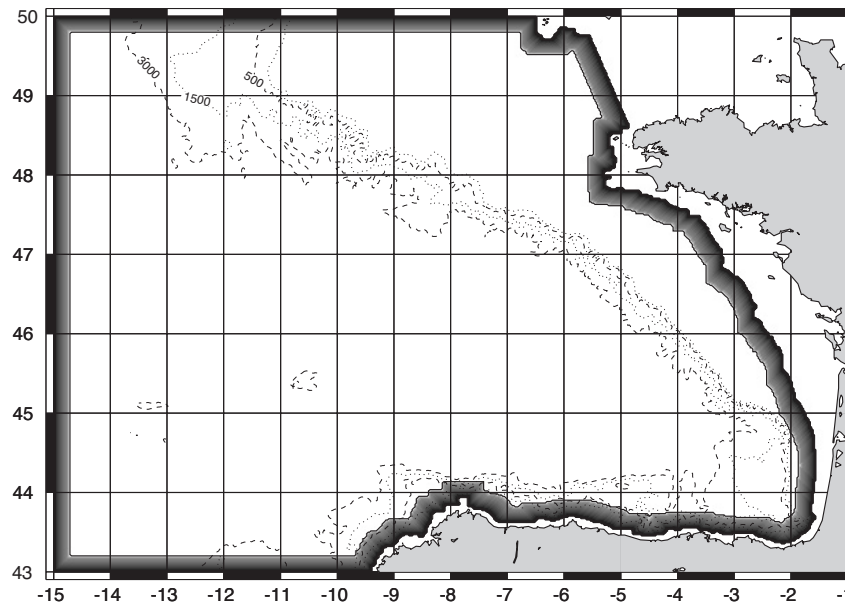


FIG. 2. – Numerical domain. Over the continental shelves, the domain is bounded by the isobath 80 m. The relaxation zone and sponge layer are over 13 grid points (i.e. ≈ 24 km).

and continuity hydrostatic primitive equations are integrated over the thickness of each isopycnic layer. Previous studies using steep topography in a stratified fluid (Smith, 1992) confirmed the validity of the numerical results near the bottom slope. The model takes into account the sea-surface variations and gives the quickest barotropic mode and the lowest baroclinic mode with a time-splitting of the equations. The focus is on propagation of internal tides, especially over the continental slope and in the deep ocean. Atmospheric momentum, heat fluxes and mixing processes are not considered. Vertical mixing generated by internal tides themselves probably affect their dissipation in a narrow band around the shelf break (Le Tareau and Mazé, 1993), and at particular locations of the Bay of Biscay (New and Pingree, 1990); in an initial approach this mixing process is supposed to not interfere with the three-dimensional distribution of the internal tide.

The grid resolution of the model is chosen for a good representation of the canyons over the French continental slopes which are areas of internal tide generation. A horizontal grid size of 1.8 km is used. Data processing from the SHOM data base leads to a smoothed bathymetry at the model resolution.

The domain is the Bay of Biscay, from 43N to 50N and from 15W to the isobath 80 m, and excludes the continental shelf close to the coast (Fig. 2). Near the coast, no internal tides of significant amplitude (compared with the ones generated over the shelf break) can be propagated from the coast to

the deep ocean. Indeed, as is described in (Serpette and Mazé, 1989), the baroclinic tide is generated by the spatial variations of the barotropic vertical velocity $\nabla\vec{H} \cdot \vec{U}$ near strong topographic accident, where ∇H is the topographic gradient and \vec{U} the barotropic horizontal tidal velocity. Near the coast, except around the Ushant Island, the barotropic tidal forcing term defined by

$$\frac{\nabla\vec{H} \cdot \vec{U}}{H}$$

is much lower than the values calculated over the shelf break. Around the Ushant Island, intensive mixing processes (Ushant front) induce homogeneous vertical density which prevents internal tide generation. In the south part of the domain, the vertical stratification induced by the Loire and Gironde estuaries may intensify the internal tides coming from the shelf break; this process is not modelled here and may locally affect the results presented on the shelf.

The model is made with four open boundaries and is forced by the main semi-diurnal tidal harmonics (M2, S2, N2, K2) from the LEGI spectral model (Le Provost, 1996). A flow relaxation scheme (Martinsen and Engedahl, 1987) is used for the barotropic prognostic variables (depth-averaged velocities and sea surface elevation) over 13 grid points close to the boundaries (see Fig. 2). The internal tide is generated inside the domain and propagated towards the boundaries. For the

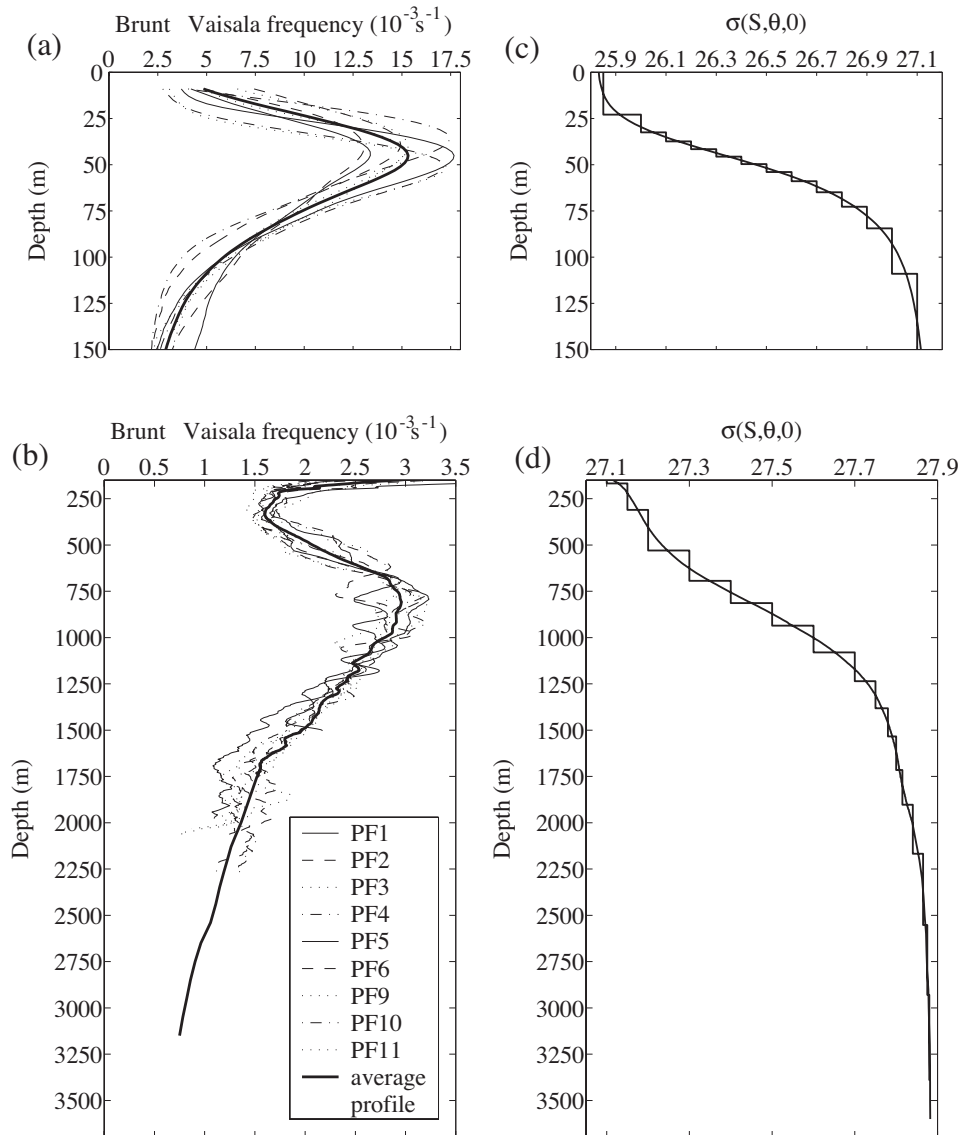


FIG. 3. – Initial density profile in September. (a-b) Brünt-Väisälä frequency, N , from 0 to 150 m depth (a) and from 150 to 3500 m depth (b). The solid bold line is the mean Brünt-Väisälä profile and the others are the tidal-cycle-averaged N profiles from stations. Inside the seasonal thermocline, there is a large dispersion of the Brünt-Väisälä frequency around the mean maximum value. (c-d) Layered vertical density from 0 to 150 m depth (c) and from 150 to 3500 m depth (d). Below 2500 m, the large layers (300 to 500 m thickness) are defined by the weak stratification ($N < 10^{-3} \text{s}^{-1}$).

baroclinic mode, radiation conditions are applied to the boundaries in order to allow wave propagation out of the computational domain. This radiation is performed by an implicit two-dimensional Orlandi condition applied to baroclinic prognostic variables (velocities and layer thickness), and is associated with a sponge layer over 13 grid points (see Fig. 2).

The barotropic and baroclinic time-step defined by the celerity of the surface tide and by the splitting method of the equations are respectively $\Delta t_{\text{trope}} = 2.5 \text{ s}$ and $\Delta t_{\text{cline}} = 150 \text{ s}$. The viscosity coefficient, ν , is a Smagorinsky viscosity eddy coefficient (it is function

of the absolute value of the total deformation of the velocity field) which is bounded by a lower limit ν_{low} when the deformation of the velocity field is weak. ν varies from $\nu_{\text{low}} = 5 \text{ m}^2 \text{ s}^{-1}$ to $\nu_{\text{max}} = 100 \text{ m}^2 \text{ s}^{-1}$ near the shelf break. The bottom friction coefficient is zero. As described in Xing and Davies (1996), the most important feature in the vertical current structure is the internal pressure gradient associated with the tide propagation; the introduction of the bottom friction only reduces the intensity of the current in a near-bed bottom layer of about 10 metres.

The model is initialised with a barotropic velocity field from the LEGI spectral model inter-

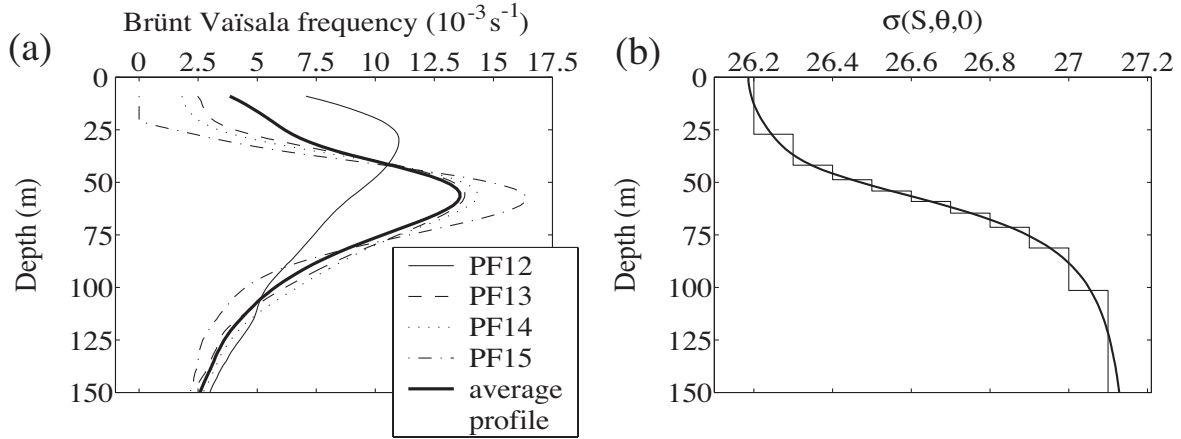


FIG. 4. – Initial density profile in October from 0 to 150 m depth. Below 150 m depth, the profile is the same as in September. (a) Brünt-Väisala frequency, N . The solid bold line is the mean Brünt-Väisala profile and the others are the tidal-cycle-averaged N profiles from stations. The mean profile is different from the PF12 and PF15 profiles. (b) Layered density profile.

polated on the MICOM grid and with no baroclinic current. The density field is initially homogeneous in the horizontal plane. Vertically, a mean density is defined from two months, September and October. In the top 2500 m, these profiles are monthly and spatially averaged from measurements collected during the MINT94 experiment. Below, an annual mean profile derived from the hydrological SHOM data base on the region is used. In Figure 3, the mean Brünt-Väisala frequency and the layered density profile are plotted for the September case: thirty isopycnal levels represent the vertical density variations of the seasonal and permanent pycnoclines and of the deep ocean stratification. In the deep layers, i.e. between 2500 and 3600 m, the Brünt-Väisala frequency varies from $1.1 \cdot 10^{-3} \text{ s}^{-1}$ to $0.5 \cdot 10^{-3} \text{ s}^{-1}$: it is lower than the value defined previously by (New *et al.*, 1988), but sufficient to allow the propagation of a semi-diurnal internal tide with a mean frequency of $1.4 \cdot 10^{-4} \text{ s}^{-1}$.

TABLE 2. – Horizontal phase speed and wavelengths of the baroclinic modes 1 to 3 at the M2 tide frequency calculated with a bottom depth typical of the French continental shelf (125 m) and with 10 layers (from 0 to 125 m depth).

Baroclinic modes	Phase speed (m s ⁻¹)	Wavelength (km)
September case		
1	0.75	33.54
2	0.30	13.41
3	0.20	8.94
October case		
1	0.66	29.51
2	0.24	10.73
3	0.17	7.60

In Figure 4, the October profiles are plotted in the upper 200 m. In deeper waters, the mean vertical density profile is quite similar to the September profile. In the seasonal thermocline, a cooling of the surface layers (i.e. an increase of the from 25.9 to 26.2) is observed between the two cases: this weak variation is a consequence of the measurement averaging. The wavelengths of the different baroclinic modes extracted from the vertical Brünt-Väisala profiles are summarised in Tables 2 and 3 to facilitate the interpretation of the model results.

MODEL RESULTS

Barotropic tide

The barotropic tide, calculated by MICOM, must be validated over areas where strong topographic variations generate the internal tides. The barotropic tide is explored in a case with no stratification. The model is run for one month to extract each semi-di-

TABLE 3. – Horizontal phase speed and wavelengths of the baroclinic modes 1 to 3 at the M2 tide frequency calculated with a bottom depth typical of the Abyssal plain (4500 m) and with 33 layers.

Baroclinic modes	Phase speed (m s ⁻¹)	Wavelength (km)
September case		
1	3.30	147.56
2	1.45	64.84
3	1.10	49.19
October case		
1	3.52	157.40
2	1.52	67.98
3	1.05	46.95

TABLE 4. – Harmonic analysis of the barotropic velocity for the data, the model and the forcing at DP94-1 and DP94-2 locations.

Tidal constituent	Semimajor axis (cm/s)	Semiminor axis (cm/s)	Orientation (deg)	Situation (deg)
<i>DP94-1 data</i>				
M2	19.56	-9.53	42.30	76.95
S2	7.93	-4.35	47.37	124.17
N2	3.40	-1.93	52.52	71.66
K2	2.27	-1.25	49.39	125.86
<i>DP94-1 model</i>				
M2	24.88	-11.88	27.81	60.01
S2	9.42	-4.33	26.74	99.55
N2	4.33	-2.05	26.57	46.98
K2	2.70	-1.24	26.59	100.17
<i>DP94-1 forcing</i>				
M2	20.98	-10.90	33.25	62.68
S2	7.44	-3.72	31.40	104.22
N2	3.93	-2.04	32.52	45.81
K2	1.94	-0.94	30.68	103.25
<i>DP94-2 data</i>				
M2	30.58	-21.97	38.40	89.88
S2	12.35	-7.49	29.13	139.36
N2	7.68	-5.59	36.01	64.41
K2	3.54	-2.14	30.83	138.73
<i>DP94-2 model</i>				
M2	36.77	-15.20	14.73	16.99
S2	15.06	-5.90	16.47	57.40
N2	6.89	-2.78	14.21	2.41
K2	4.32	-1.69	18.89	57.16
<i>DP94-2 forcing</i>				
M2	14.79	-7.41	27.42	19.99
S2	5.65	-2.61	26.58	60.52
N2	2.90	-1.46	28.00	2.12
K2	1.53	-0.69	26.98	59.78

The orientation of the major axis is counted clockwise from 0 degree in the Northward direction. The situation is the phase lag referenced to UT+0.

urnal tidal component by harmonic analysis. At DP94-1 and DP94-2, the modelled barotropic tidal current is compared with the depth-averaged velocity calculated from ADCP observations (see Table 4 and Fig. 5). At DP942, located at the edge of a canyon, the barotropic velocity is higher than at DP941, in the model results and in the data. This difference of amplitude in the alongslope direction will induce a spatial variability of the internal tides generated near the shelf break, which justifies the use of a three-dimensional model. At DP94-1, for the M2 and S2 harmonics, the model overestimates the semi-major axis (bias of 5.3 cm s⁻¹ for M2) and the semi-minor axis (bias of 2.3 cm s⁻¹ for M2) of the tidal ellipses. At DP94-2, the semi-major axis is overestimated (bias of 6.2 cm s⁻¹ for M2) while the semi-minor axis is underestimated (bias of 6.8 cm s⁻¹ for M2). Locally the bathymetric gradient is north-south for both locations. The current ellipses is more cross-shelf oriented in the model than in the data, with a difference of 15 to 25° at DP94-1 and 12

to 24° at DP94-2. The bias in the phase lag expresses a mean phase difference of 45 min and 2 h 45 min at DP94-1 and DP94-2 respectively. At DP94-2, the M2 ellipses properties express a cross-isobath predicted current (37 cm s⁻¹) that is slightly stronger than the observations (30 cm s⁻¹), while the modelled along-isobath component (-15 cm s⁻¹) is weaker than the observations (-21 cm s⁻¹). These differences between the model and the data, particularly in the cross-shelf current and in the orientation of the ellipses, have an effect on the internal tides through the generation term (Fig. 5). However, the tidal velocity calculated by MICOM fits better to the observations than the tidal forcing used as the initial condition, which is very weak at DP94-2 (for the M2 wave, the semi-major and semi-minor axis are 15.0 cm s⁻¹ and -7.4 cm s⁻¹). These results show that the amplitude of the velocity is very sensitive to the local topography resolution. Therefore, even if there are still differences between the model and the data, the fine mesh of MICOM compared to the coarse

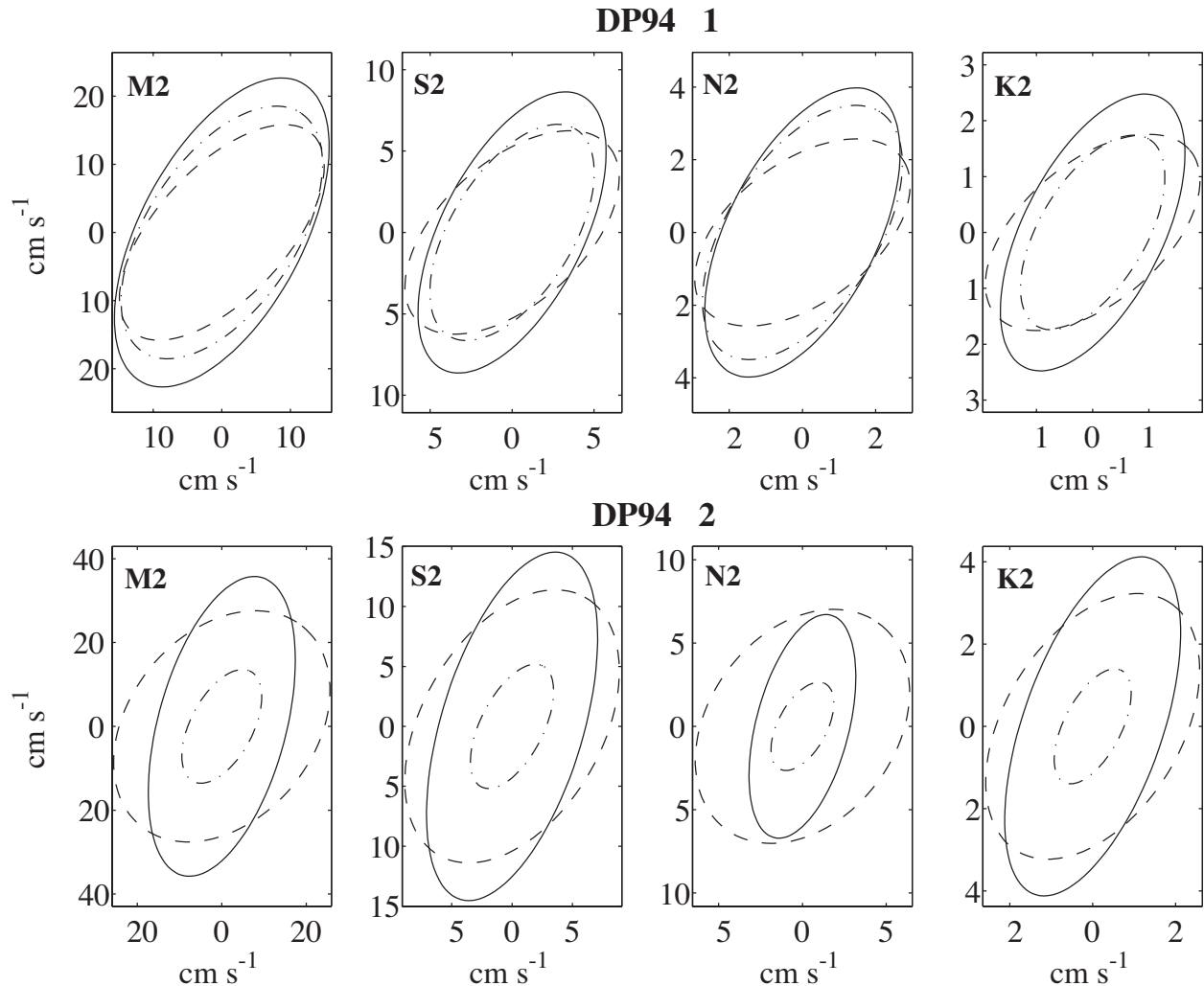


FIG. 5. – Barotropic tidal ellipses at DP94-1 and DP94-2, comparison between observation (dashed lines) and the model (solid lines); the velocity issued from the LEGI spectral model is plotted in dash-dotted lines.

grid of the spectral model (Le Provost *et al.*, 1996) used to force the model at the boundaries, and in initial conditions, improves the barotropic calculation. The discrepancies between the model and the observations, particularly in the phase of the tidal velocity, linked to the propagation of the surface tide, are probably due to the tidal forcing conditions. The effect of the internal motion on the depth mean flow is not considered since comparison is made in a weak stratification case (the data were collected in May and June, Perenne and Pichon, 1999). However, as described in Xing and Davies (1998b), even in a winter stratification case, a significant improvement of K1 and O1 velocities was found when internal motion was included. The feedback effect of the semi-diurnal internal tides on the depth-averaged velocity in such stratification cases will be explored in future studies.

Baroclinic tide

In the Bay of Biscay, two main generation areas are defined with a barotropic tidal forcing term greater than 10^{-5} s^{-1} and given by

$$\frac{\nabla \dot{H} \cdot \dot{U}_{M2}}{H}$$

These areas are located over the French shelf break (Fig. 6a) and the Spanish continental slope (Fig. 6b). They are characterised by strong bottom slope variations, such as canyons (Fig. 6a) or capes (Fig. 6b). Near the French shelf break, maximum values of the forcing term are located at the top of the different canyons; this induces an inhomogeneous distribution of the internal tides in the along-slope direction and probably interferes in their three-dimensional propagation. The maximum barotropic

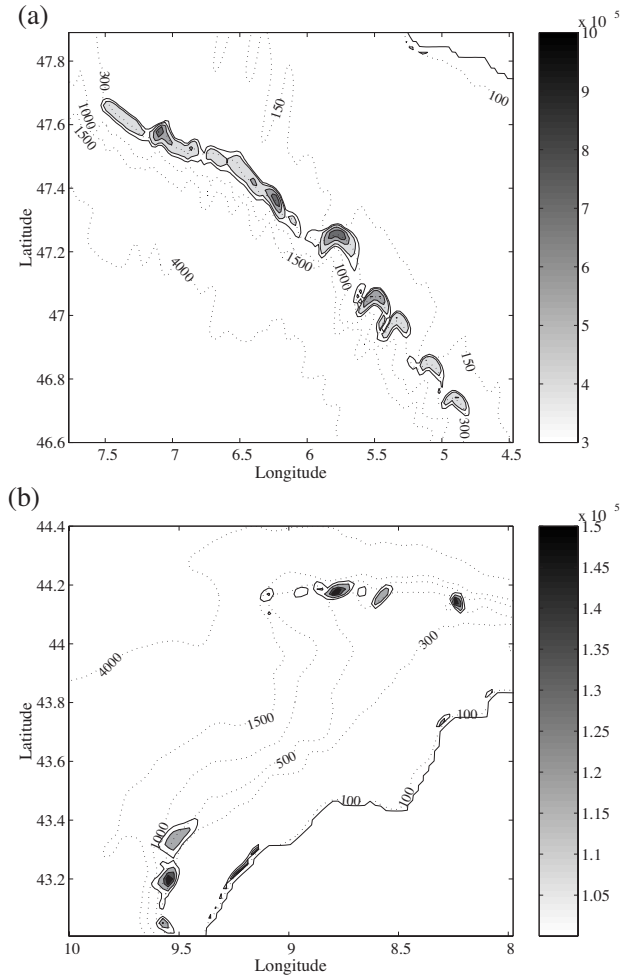


FIG. 6. – Local topography and tidal forcing term, $U \cdot \nabla H / H$ where $U \rightarrow$ is the barotropic tidal current for the M2 wave and H is the bottom depth. (a) Over the French continental shelf, isocontours are 3.10^{-5} , 4.10^{-5} , 6.10^{-5} , 8.10^{-5} s^{-1} . The maximum values situated at depth of 300 m, between 5.5 and $7.5^{\circ}W$, defines the main generation areas. (b) Over the Iberian continental slope, isocontours are 1.10^{-5} , $1.2.10^{-5}$, $1.4.10^{-5}$ s^{-1} . The maximum values are situated at depths of between 500 and 1000 m at the north edge of the Ortelgal Cape ($44.2^{\circ}N$ and 8.5 to $9^{\circ}W$).

forcing value ratio between the Iberian continental slope ($1.4 \cdot 10^{-5} s^{-1}$) and the French continental slope ($8 \cdot 10^{-5} s^{-1}$) is nearly 1/5. The internal tide generated in these two areas is characterised by vertical variations of isopycnals (with associated vertical and horizontal shears of currents) at tidal frequencies; then, the forced internal waves, generated in the areas described hereabove, take a few days to propagate inside the domain at different wave speeds defined by the baroclinic modes (Tables 2 and 3). The model is run over a period of 21 days, the initial baroclinic current being zero. The time needed by the baroclinic modes (see the wavelengths in Tables 1 and 2) to reach the limit of the domain corresponds to a transient state. The internal tide generation process is

not the goal here, so we present the model results after this transient state.

Hereafter, the three-dimensional propagation of the internal tide over the abyssal plain is firstly described by horizontal variations of the surface baroclinic velocity. Then, the objective is to point out the correlation between these horizontal variations and the vertical internal tide propagation along a particular section S. This section is chosen to represent the steep topography theoretical case as well as possible (Baines, 1982).

The spatial variations of the east-west surface baroclinic current after the Spring tide of September is plotted in Figure 7a. All baroclinic modes are propagated after 12 days of simulation: the model shows variations of surface baroclinic currents from -20 to $+20$ $cm s^{-1}$ at the different baroclinic wavelengths of the internal tide. Indeed, successive positive and negative values are significant of the internal tide propagation. The most intense velocities correspond to the $45/47^{\circ}N$ and $6/8.5^{\circ}W$ region, and are due to the maximum values of the barotropic tidal forcing term between 6.5 and $7.5^{\circ}W$ near the French shelf break (Fig. 6a). The intense velocities observed in the south part of the model are produced by an internal tide generated over the Iberian continental slope by $8.6^{\circ}W$, $44.2^{\circ}N$ (Fig. 6b). The spatial distribution of the surface velocity and particularly the maximum negative values simulated around $7^{\circ}W$ - $46.7^{\circ}N$ and $7.5^{\circ}W$ - $45.6^{\circ}N$ are directly correlated with the propagation of the internal tide in the vertical plane. This can be explained by an example of the vertical distribution of the internal tide amplitude (Fig. 7b) and of the east-west baroclinic velocity (Fig. 7c) along S. The section S, perpendicular to the French continental slope, is chosen at the northern edge of the most energetic area (45 - $47^{\circ}N$, 9 - $6^{\circ}W$) in order to avoid the influence of the internal tides coming from the Iberian continental slope. The internal tide amplitude is defined by the amplitude of the interface elevation at the mean semi-diurnal frequency corresponding to the four tidal waves M2, S2, N2, K2, averaged over five tidal cycles around the spring tide. In Figure 7b, the maximum internal tide amplitude follows the slope of the characteristic rays. In the non-hydrostatic case, the slope of the rays is defined as

$$c(z) = \left(\frac{w^2 - f^2}{N^2(z) - w^2} \right)^{1/2},$$

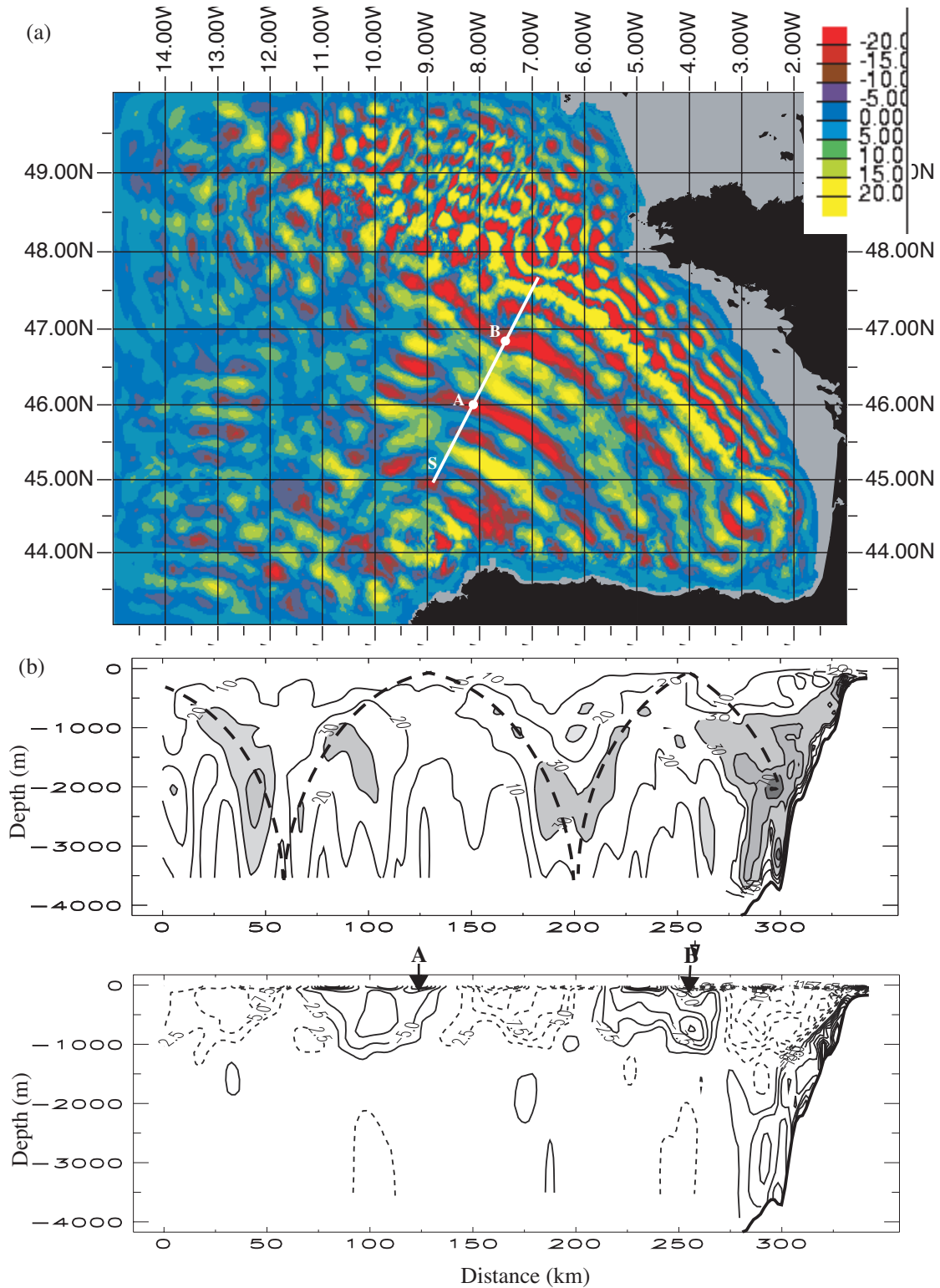


FIG. 7. – (a) Modelled east-west surface baroclinic velocity in September on 09/09 at 19 h (after the spring tide). Over the abyssal plain, velocity varies from -20 cm s^{-1} (red) to $+20 \text{ cm s}^{-1}$ (yellow). Over the continental shelf, maximum values reach $\pm 50 \text{ cm s}^{-1}$ at different areas (around $7^\circ\text{W } 48^\circ\text{N}$ and $5.5^\circ\text{W } 47.25^\circ\text{N}$); 50 km from the shelf break maximum values of the baroclinic current reach $\pm 30 \text{ cm s}^{-1}$. (b) Distribution of the internal tide amplitude along section S from $8.9^\circ\text{W } 45.0^\circ\text{N}$ to $6.9^\circ\text{W } 47.6^\circ\text{N}$. The amplitude is the Fourier coefficient of the model result at the mean frequency of the four tidal waves, calculated over five tidal cycles. The bold dashed lines represent the paths of the characteristic rays. (c) Evolution of the total across-slope velocity along section S on 09/09 at 19 h. The angle between the normal to the bottom slope and the north is 25° . Dotted lines are negative values, dashed lines are positive values.

where w is the tidal frequency, f the Coriolis parameter and $N(z)$ the buoyancy frequency (New, 1988). With the equations of the MICOM model where the hydrostatic approximation is applied it becomes

$$c(z) = \left(\frac{w^2 - f^2}{N^2(z)} \right)^{1/2}.$$

Between 200 m and 2000 m, this slope is lower than the local bottom slope and the internal tide energy sweeps along the downward ray before being reflected. Over the abyssal plain, the reflection on the bottom depth, H , occurs every 150 km (the first downward ray is reflected at about 200 km and the second one at 50 km, Fig. 7b). This distance is close to the wavelength of the first baroclinic mode (Table 3). Indeed, the dispersion relation of the internal waves defined in the linear theory, with a constant Brünt-Väisälä frequency and a flat bottom, yields the ratio between the vertical mode $m_j = j\pi/H$ and the horizontal wavenumbers, k_j , of the mode j :

$$\frac{m_j}{k_j} = \left(\frac{w^2 - f^2}{N^2(z)} \right)^{1/2}.$$

For the first baroclinic mode, $m_1 = \pi/H$,

$$\lambda_1 = 2H \cdot \left(\frac{w^2 - f^2}{N^2(z)} \right)^{1/2},$$

and λ_1 is proportional to the ray slope $c(z)$.

In Figure 7c, strong negative values of the east-west baroclinic current in the upper layers (point A, B) are correlated with the resurgence of the internal tide coming from the deep ocean. The first and second maximum current areas located 100 and 250 km from the south end of the section S correspond to the maximum negative values of Figure 7a. The distance between these two maximums corresponds to the baroclinic first mode wavelength (points A and B of the section S on Fig. 7a).

In conclusion, over the abyssal plain, the spatial distribution of the east-west surface baroclinic velocity, and particularly the horizontal shears within the most intensive area, are induced by the propagation of the main baroclinic modes. These initial results show that the propagation of the internal tide in the deep ocean has an influence on the distribution of the current in the upper layers.

The propagation of the internal tide over the French continental shelf has already been modelled

(Serpette *et al.*, 1989). We focus here on the values of the surface baroclinic currents in the north part of the French continental shelf, between 47 and 49°N. In this realistic simulation, they reach more than 50 cm s⁻¹ at locations where wave interferences are constructive (nodes and anti-nodes are due to the orientation of the bottom continental slope, which is different between 46.5 and 47.5°N and between 47.5 and 48.2°N, but are also due to canyons characterised by maximum forcing term values (Fig. 6a). These high baroclinic velocities probably have an effect on the meso-scale circulation on the continental shelf.

In the following parts, we focus on the model results along sections in which data were collected during the Mint94 experiment: the model outputs are presented along the two vertical sections S1 (PF01-PF05), S2 (PF06-PF10) for the September case and section S3 (PF11-PF15) for the October case (see Fig. 3). In this last case, the distribution of the horizontal tidal current is also briefly compared with that of the September case. In the sections, the internal tide amplitude has the same definition as in section S. The total across-slope current is the baroclinic velocity plus the depth-averaged velocity projected in the direction perpendicular to a bottom slope defined locally between the 200 and 1000 m isobaths.

The September stratification case

Section S1

In Figure 8a, the vertical distribution of the maximum internal tide amplitude along the characteristic rays is not as clear as in section S (Fig. 7b). In addition to the shelf break topographic variations, strong bottom slope variations (at about the 80 km position) are due to the Meriadzeck Terrace. These variations induce other generation areas at the two edges of this topographic feature, at a depth of about 2500 m. Internal tide amplitude maximums are located between 2000 and 3000 m around the Meriadzeck Terrace and vary from 50 to 70 m in the spring tide. The PF04 position is also located in this area. Along S1, three waves are generated and interact. Two waves generated near the shelf break and at the 75 km position are in phase, whereas the third one, generated at 100 km, is in opposition with the others. In Figure 8b, the instantaneous interface elevations confirmed this difference in phase. The interface elevations are positive for the first two

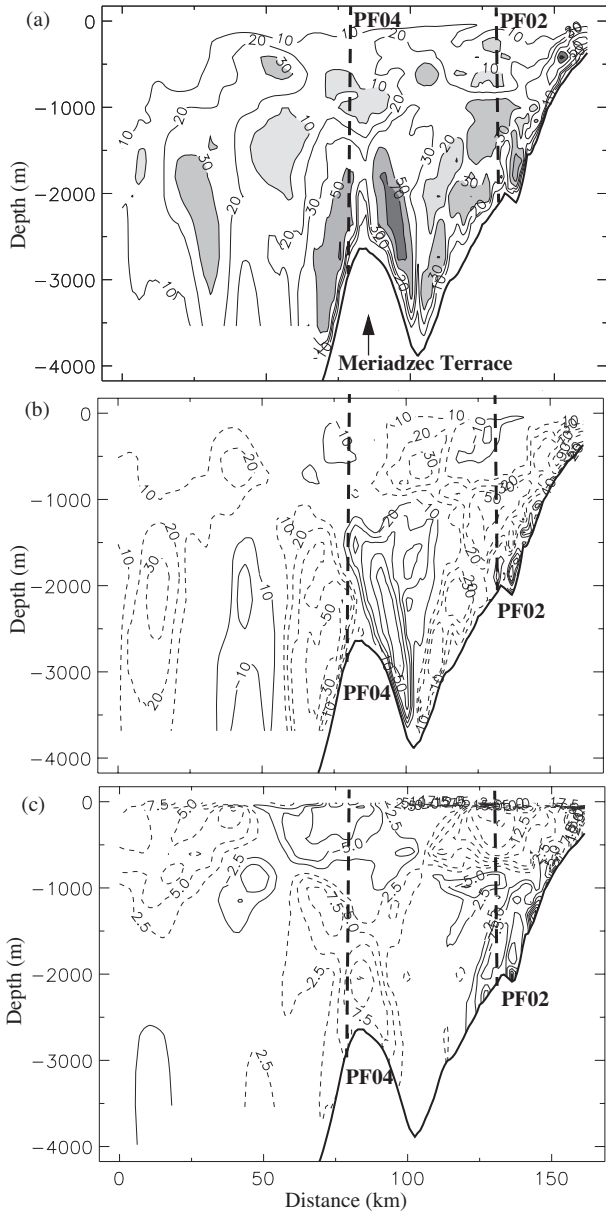


FIG. 8. – (a) Distribution of the internal tide amplitude along section S1 from 9.5°W 46.9°N (PF05) to 8.5°W 48.10°N (close to DP941), calculated as for section S (Fig. 7b). (b) Distribution of the interface elevations along S1 on 09/09 at 19 h (the same tidal hour as for Fig. 7). (c) Distribution of the total across-slope velocity along S1 on 09/09 at 19 h. The angle between the normal to the bottom slope and the north is 30°. Dotted lines are negative values, dashed lines are positive values. The two bold shaded lines are the PF04 and PF02 locations.

waves and negative for the third one. In Figure 8c, the vertical distribution of the total across-slope velocity is correlated with the variations in the interface elevation. The maximum values, from 8 to 10 cm s⁻¹, are confined above the Meriadzeck Terrace at about 2200 m depth. Elsewhere on the section, the maximum horizontal velocity values are located between 0 and 2000 m. This vertical veloci-

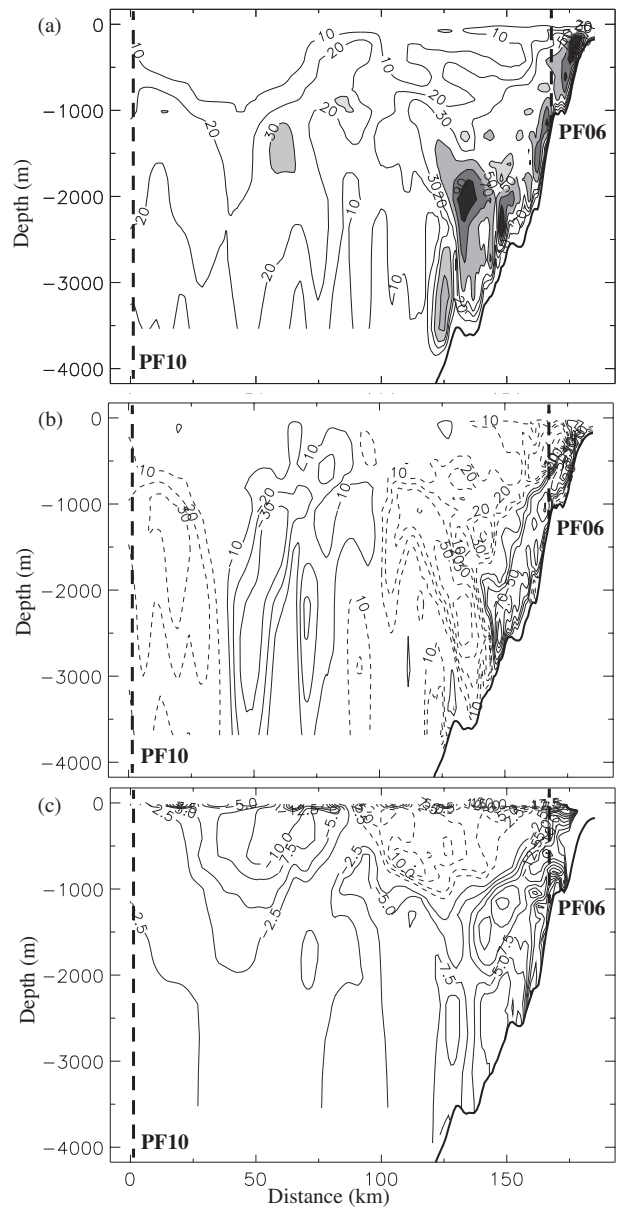


FIG. 9. – (a) Distribution of the internal tide amplitude along section S2 from 8.23°W 46.25°N (PF10) to 7.0°W 47.6°N, calculated as for section S (Fig. 7b). (b) Distribution of the interface elevations along S2 on 09/09 at 21 h. (c) Distribution of the total across-slope velocity along S2 on 09/09 at 21 h. The angle between the normal to the bottom slope and the north is 25°. Dotted lines are negative values, dashed lines are positive values. The bold shaded line is the PF06 location.

ty distribution (already observed in section S) is a consequence of the vertical density profile used in the model. Indeed, the buoyancy frequency N , greater than $1 \cdot 10^{-3} \text{ s}^{-1}$ between 500 and 2500 m (with a maximum value of $2.8 \cdot 10^{-3} \text{ s}^{-1}$ at 800 m due to the Mediterranean water), decreases from $1 \cdot 10^{-3} \text{ s}^{-1}$ to $0.5 \cdot 10^{-3} \text{ s}^{-1}$ between 2500 m depth and the bottom (Fig. 3). These values, which are larger than the

mean frequency of the tidal wave ($1.4 \cdot 10^{-4} \text{ s}^{-1}$), allow a propagation of the internal tide in the whole water depth. However, the maximum horizontal velocity values are concentrated above 2500 m depth, where the vertical stratification and therefore the horizontal pressure gradients are great. Inversely, the maximum values of interface elevations (i.e. the vertical velocity) are concentrated in the bottom layers where the buoyancy frequency is weak. Along S1, the velocity is in phase opposition every 75 km and in phase every 150 km, as it is in section S (Fig. 7c). This confirms the main influence of the first baroclinic mode. In the vertical, this influence is characterised by a vertical shear of current which occurs at mid-depth at point PF02.

Section S2

In Figure 9a, the internal tide amplitude plotted along section S2 exceeds 90 m near the bottom depth at the PF06 location. This is due to the characteristic ray slope which is very close to the bottom slope and therefore near the critical value (Baines 1982; Jezequel *et al.*, 2002). The reflection of the characteristic ray occurs at the bottom depth (3000 m). The maximum value of the internal tide amplitude decreases as the wave propagates over the

abyssal plain. A part of this damping is due to the propagation of the baroclinic spring-neap tidal wave. The internal tide amplitude is an average of the interface elevation around the spring tide of the sea surface at the shelf break. Since the model is forced by the four main semi-diurnal waves, different tidal frequencies propagate at different wave speeds. Particularly, the baroclinic spring-neap tidal waves need several days to propagate from the generation area. Therefore, if the baroclinic spring tide is in phase with the spring tide of the sea surface near the shelf break, this is not the case 180 km (PF10) from the generation area. The damping of the amplitude is also due to the dissipation introduced in the model by the different viscous coefficients. In Figure 9b, the instantaneous interface elevation plotted after the spring tide decreases by 40% at 70 km (the maximum values decrease from 50 m at 120 km to 30 m at 50 km). In Figure 9c, the total across-slope current is plotted at the same time as in Figure 9b. The modelled maximum values are 10 to 15 cm s^{-1} in the layers near the sea surface at about 75 km, i.e. where the characteristic ray coming from the deep ocean encounters the sea surface. There is a transfer between the vertical velocity (which is zero in the top layers at 75 km, see Fig. 9b) and the horizontal velocity.

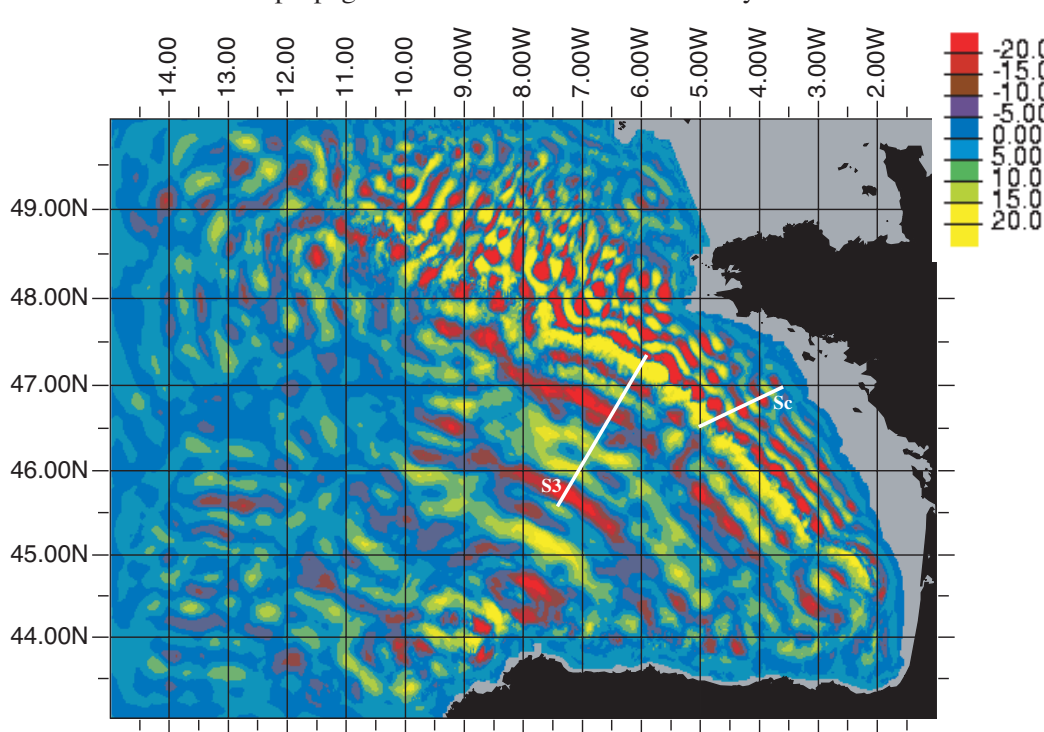


FIG. 10. – Modelled east-west surface baroclinic velocity in October on 06/10 at 6 h (before the spring tide). Over the abyssal plain, velocity varies from -20 cm s^{-1} (red) to $+20 \text{ cm s}^{-1}$ (yellow). Over the continental shelf, maximum values reach $\pm 40 \text{ cm s}^{-1}$ at different areas (around $7^\circ\text{W } 48^\circ\text{N}$ and $5.5^\circ\text{W } 47.25^\circ\text{N}$); 50 km from the shelf break maximum values of the baroclinic current reach $\pm 25 \text{ cm s}^{-1}$.

October stratification case

Figure 10 shows the east-west surface baroclinic currents in the October case, which are weaker than in the September case (Fig. 7a). Within the main wave propagation area, the maximum current has a value of 15 cm s^{-1} in the October case while it reaches 20 cm s^{-1} in the September case. Indeed, the results of October and September are respectively shown before and after the spring tide. Nevertheless, the spatial distribution of the baroclinic current is the same in both cases (Fig. 7a and Fig. 10), considered at the same hour of the semi-diurnal tidal cycle. In fact, the difference between the two buoyancy frequency profiles in the upper layers is not large enough to drastically modify the position of the horizontal current shears modelled at mid-bay (see Section 2.2 and Figs. 3a and 4a). Over the French continental shelf, the variations of the seasonal thermocline density gradient between September and October slightly modify the wavelength of the internal tide. Along section Sc (see Fig. 10), the internal tide wavelength extracted from the model output (not seen here) decreases from 33.5 km in September to 30 km in October. This variation is in good agreement with the calculation of the first baroclinic mode wavelengths with a bottom depth of 125 m, i.e. over the continental shelf (see Table 2). Over the abyssal plain, the wavelength of the third baroclinic mode, defined by the seasonal thermocline density gradient decreases from 50 to 45 km (see Table 3 and Figs. 7 and 10).

In Figure 11a, the internal tide amplitude before the spring tide is plotted along section S3, where data were collected in October. The maximum internal tide amplitudes can reach more than 50 m at mid-bay at 2000 m depth. This high amplitude compared with the other sections (S1, S2) is associated with the maximum forcing term area (see Fig. 6a). In Figure 11b, the spatial distribution of the interface elevation plotted at a particular tidal time is globally the same as in section S (Fig. 7b). However, the maximum interface elevation does not exactly follow the slope of the characteristic rays. At mid-depth, there are successive maximums of the interface elevations, spaced at about 60 km. These are due to a wave reflected on the Iberian continental slope. Indeed, at the same hour of the tidal cycle, the internal tide along the French continental slope is in phase opposition compared with the wave reflected on the Iberian continental slope. Therefore, the energies of

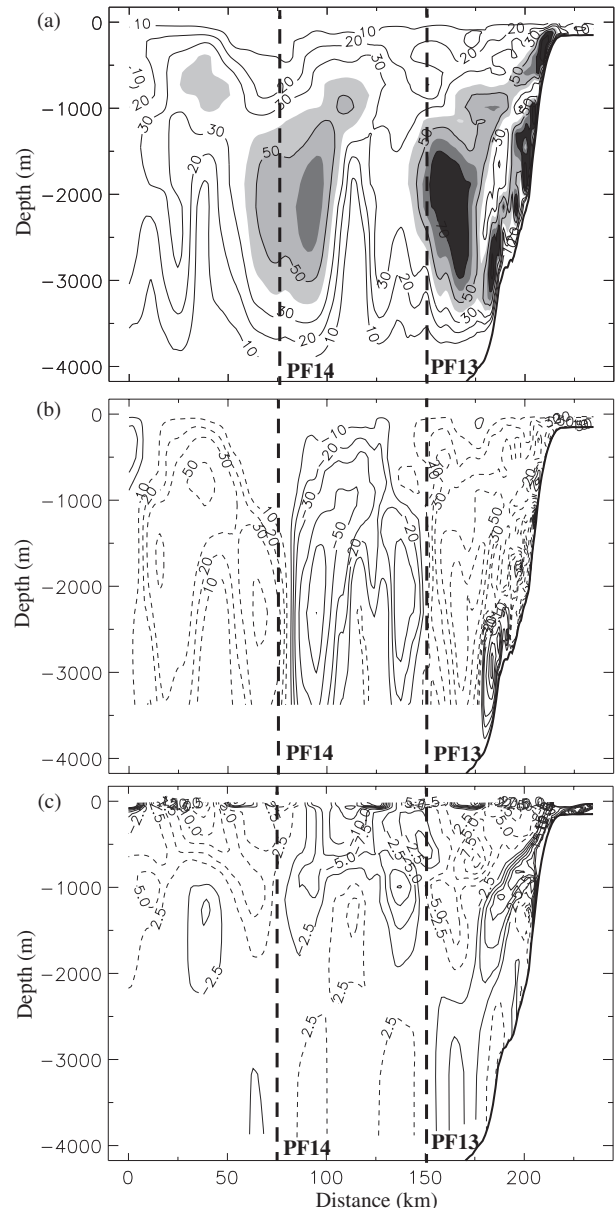


FIG. 11. – (a) Distribution of the internal tide amplitude along section S3 from $7.32^{\circ}\text{W } 45.66^{\circ}\text{N}$ (PF15) to $5.8^{\circ}\text{W } 47.4^{\circ}\text{N}$ (close to DP942), calculated as for section S (Fig. 7b). (b) Distribution of the interface elevations along S3 on 06/10 at 6 h (the same tidal hour as for Fig. 10). (c) Distribution of the total across-slope velocity along on 06/10 at 6 h. The angle between the normal to the bottom slope and the north is 16° . Dotted lines are negative values, dashed lines are positive values.

the incident and reflected waves have the same distribution along the characteristic rays only if the distance between the two continental slopes is equal or close to $n \cdot \lambda_1 + \lambda_1/2$ (where λ_1 is the first deep ocean baroclinic wavelength and n an integer). In our case, in which layers are defined from 0 to 4000 m depth, the distance between the two continental bottom slopes is 350 km. Therefore, with $\lambda_1 \approx 157 \text{ km}$ (see Table 3), we are not exactly in a constructive inter-

ference case between the two continental slopes. In Figure 11c, the spatial distribution of the total across-slope velocity shows particularly well the resurgence area in which the top layer velocities are intensified by the internal wave coming from the deep ocean. In these stratification conditions, this area is situated about 100 km from the shelf break.

DATA/MODEL COMPARISONS

All data collected during the experiment are not presented here: we have chosen to focus on the measurements located in sections S1, S2 and S3 and well phased with the Spring tidal cycle, i.e. where the internal tide is well observed. The measured internal tide amplitude is estimated via the level depth of isopycnals calculated from the density profiles. For each isopycnal level, referenced on the “z” axis to its time-averaged level, Fourier coefficients at the tidal frequency of the main wave (M2) are calculated for different samples covering one tidal period. Then, the internal tide amplitude is estimated by an average of these Fourier coefficients. The data were collected only for 25 hours, at a particular time of the spring to neap tidal cycle; therefore, this estimation represents the influence of all semi-diurnal waves. The internal tide phase is marked out in time by the maximum level depth of each isopycnal. To achieve the comparison, the same data processing is applied on the modelled density profiles. The influence of the internal tide on the velocity structure is represented by the baroclinic velocity, which is defined in both cases (data and model) by the difference between the total current and the depth-averaged current.

September stratification case

Section S1

Section S1 includes velocity and density measurements available at PF02 and PF04. The north-south baroclinic velocity is used for the data/model comparison. Its north-south orientation is close to the orientation of the across-slope component (near the shelf break, the orientation of the normal component to the bottom of the continental slope is 10° from north, while its the mean orientation along the section is 30°). In Figure 12, the modelled and observed baroclinic component time evolution are

displayed for PF02. This station over the French continental slope includes measurements down to 2300 m depth (see Table 1). The temporal variation of the velocity, nearly in phase in the model (Fig. 12a) and in the data (Fig. 12b), follows the semi-diurnal tidal cycle. Maximum values of the baroclinic current reach 8 cm s^{-1} in the model, and 12 cm s^{-1} in the observations. These values validate the influence of the internal tide propagation on the velocity structure. Indeed, the barotropic tidal current (due to the surface tide) is only 3 cm s^{-1} for a water depth of 2400 m (the data were collected 5 days before the spring tide: see Table 1). Nevertheless, the model result is weaker than the observed velocity, probably due to the viscosity of the model, which was slightly too high. The other main feature is the good agreement between the modelled and observed phase differences in the vertical: this vertical shear of baroclinic current above the continental slope is the result of the propagation of the internal tide in the vertical plane (see the model result of the across-slope current along section S1, Fig. 8c). However, the depth of the vertical

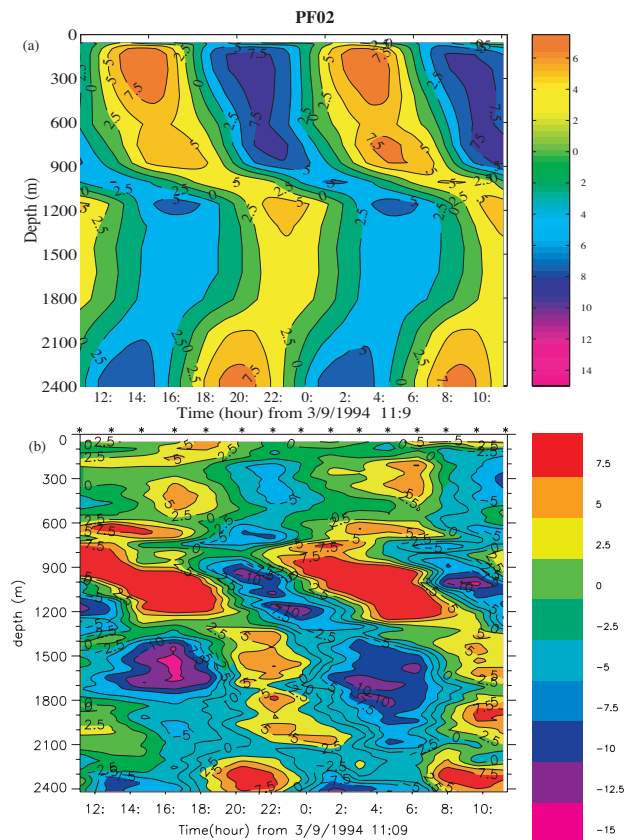


FIG. 12. – Time series of north-south baroclinic velocity at the PF02 location from the model (a) and from lowered ADCP measurements (b) during two semi-diurnal tidal cycles (25 hours).

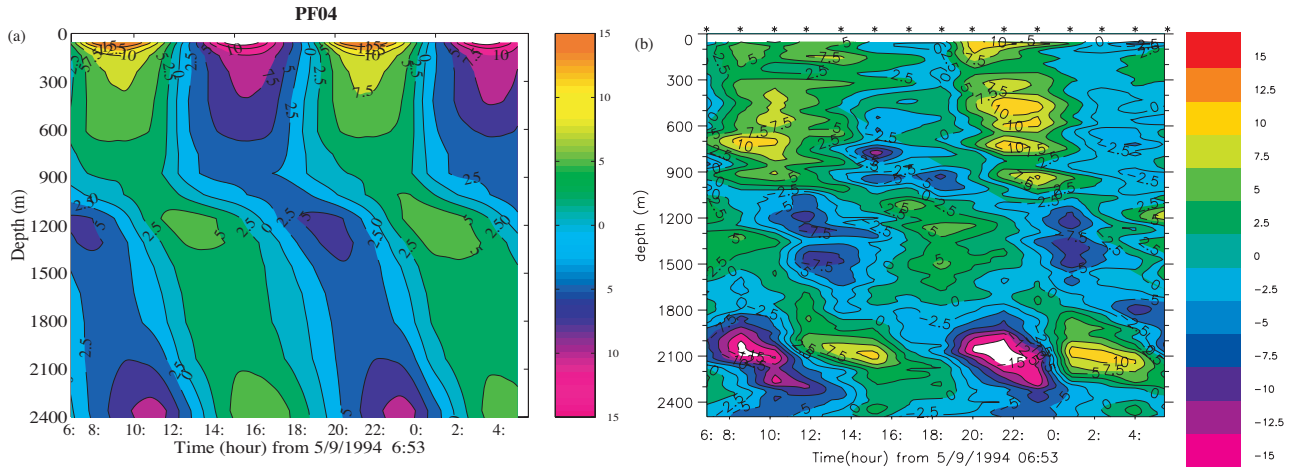


FIG. 13. – Time series of north-south baroclinic velocity at the PF04 location from the model (a) and from lowered ADCP measurements (b) during two semi-diurnal tidal cycles (25 hours).

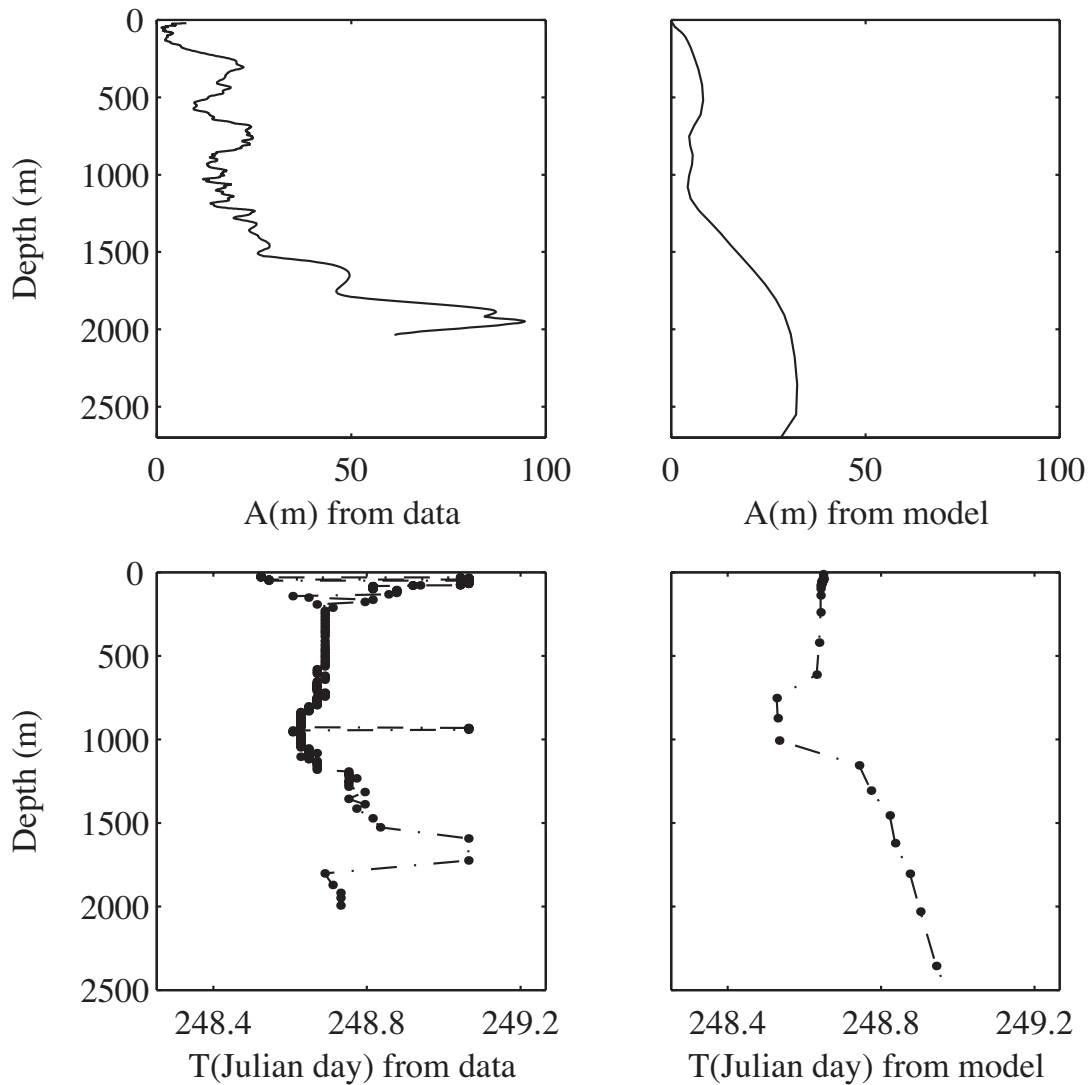


FIG. 14. – Vertical distribution of the estimated amplitude (A) and of the phase (T) of the internal tide from the model and from the observations at PF04 location. The calculation of A is detailed in *Data/model comparisons* Section. T is the moment, in Julian day, when the internal tide trough crosses over PF04.

current shear is not exactly the same in the data (1400 m) and in the model (1000 m). The model water depth is directly correlated to the characteristic ray slope, which depends on the vertical stratification introduced as initial conditions. Therefore, an improvement of the model result could be achieved by introducing three-dimensional variations in the initial density field.

In Figure 13, the time evolutions of the modelled and observed baroclinic component are displayed for PF04. This point, further offshore than PF02, is located at the south edge of the Merriadzeck Terrace (see Fig. 1 and Fig. 8b). In both cases, the baroclinic velocity follows the semi-diurnal tidal cycle (Figs. 13a and 13b), but the data are much noisier than the model result. The observed and modelled vertical current shears are in nearly good agreement only between 20 and 24 h. The main feature here is the increase in the velocity near the deepest level, at 2400 m, in the model as well as in the data: maximum values can reach more than 20 cm s^{-1} in the observations. In the model result along section S1 (Fig. 8), this velocity increase near the deepest level is easily explained by the generation area located near the point PF04.

In Figure 14, the vertical distribution of the internal tide (amplitude and phase as defined here above) is plotted at the point PF04. The main feature is the increase in the internal tide amplitude at a water depth of 2000 m, which is observed in the data and in the model result. This increase in the internal tide amplitude in the near-bed layers is probably due to an upward ray coming from the south edge of the Merriadzeck Terrace (see Section 3.2). The magnitude of the internal tide elevation modelled by MICOM can reach about 50 m (see section S1, Fig. 8b); it is lower than in the data, where a peak of about 90 m is observed at 2000 m. In the time variations, there is a delay of about 0.2 days (see the vertical distribution of the phase) between the model and the data. A poor definition of each forcing term (topography, surface tide, density) could be evoked to explain this delay. PF04 is close to strong topographic variations; therefore, a bad definition of very fine topographic structures involving other generation locations could explain this difference rather than a bias in the initial density structure.

Along section S1, the vertical current shear modelled at PF02 and the existence of several generation areas, particularly near the Merriadzeck Terrace (PF04), are confirmed.

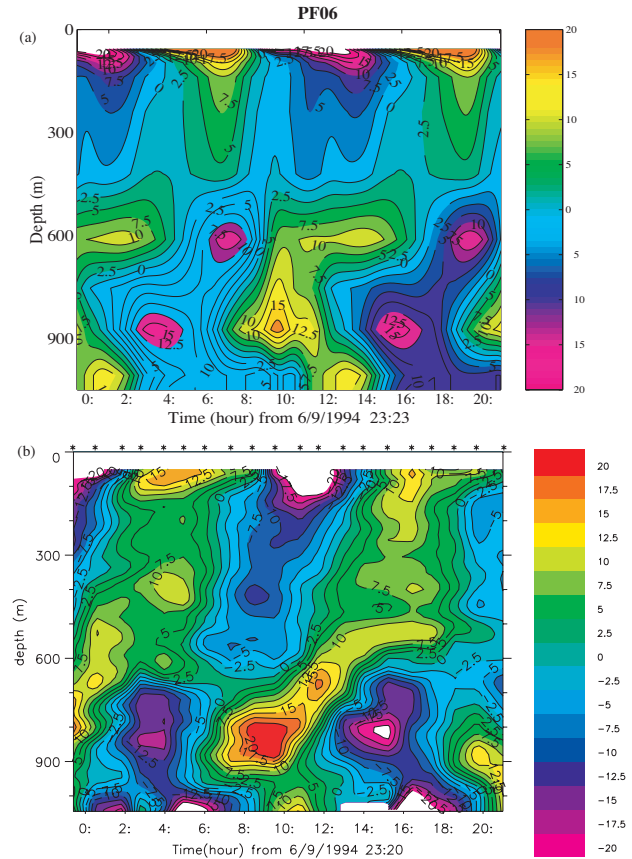


FIG. 15. – Time series of north-south baroclinic velocity at the PF06 location from the model (a) and from lowered ADCP measurements (b) during two semi-diurnal tidal cycles (25 hours).

Section S2

Along section S2, the main objective is to confirm by the observations the modelled vertical current shear and the increase in the internal tide amplitude in the near-bed layers of the continental slope.

In Figure 15, the time evolution of the north-south baroclinic velocity is plotted at PF06. This point is located over the French continental slope at a water depth of 1100 m (see Table 1). As for PF02 and PF04, the time evolution of the velocity follows the semi-diurnal tidal cycle. The agreement between the model result (Fig. 15a) and the data (Fig. 15b) is nearly good, with a phase difference of about two hours, probably due to the bias on the predicted barotropic current (see *Barotropic tide* Section in *Model results*). The vertical phase opposition, i.e. the vertical current shear, is particularly well modelled between 50 and 1000 m. Near the sea-surface, the data collected by the lowered ADCP are not available. The modelled vertical current shear due to the seasonal thermocline cannot be confirmed. In

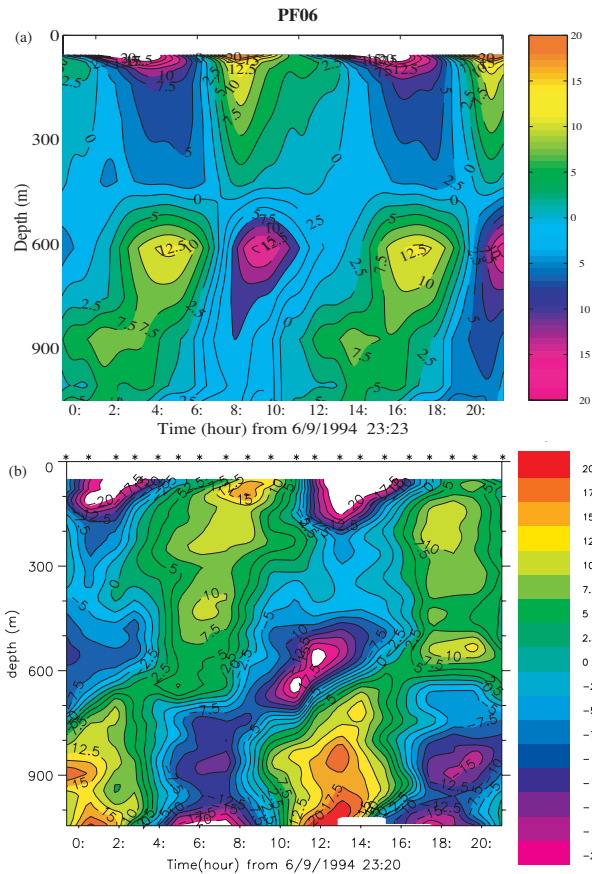


FIG. 16. – Time series of east-west baroclinic velocity at the PF06 location from the model (a) and from lowered ADCP measurements (b) during two semi-diurnal tidal cycles (25 hours).

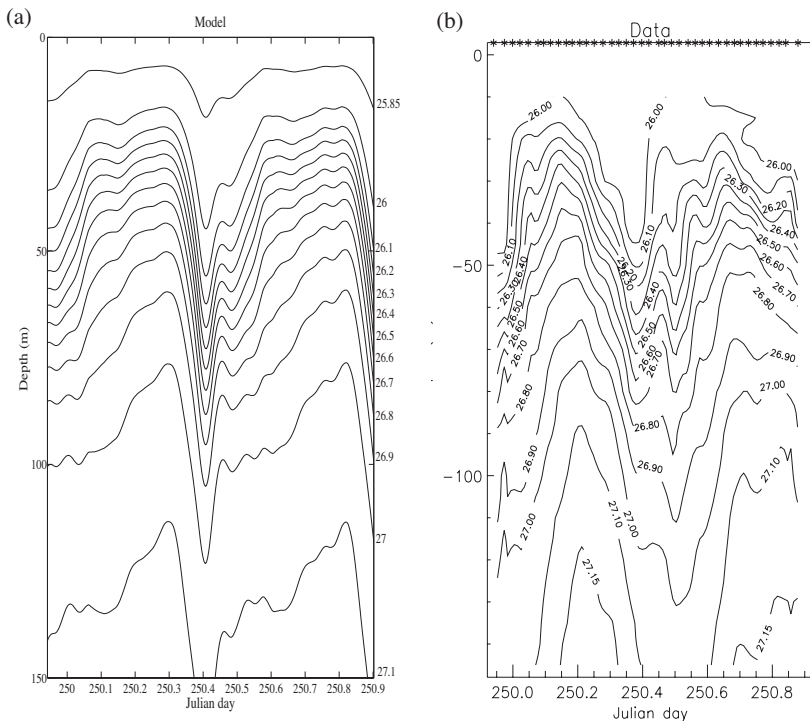


FIG. 17. – Time evolution of isopycnal interfaces from the model (a) and of isopycnal depths from CTD stations between 0-150 m depth (b), during two semi-diurnal tidal cycles at the PF06 location.

the near-bed layers, the predicted current (15 cm s^{-1}) is slightly weaker than the measured current (20 cm s^{-1}), which is an effect of the model viscosity.

The time evolution of the east-west baroclinic component plotted in Figure 16 at the same location, PF06, confirms the previous result. In the data, there is an advance in phase of the velocity in the near-bed layers compared to the velocity in the near-surface layers. This is in agreement with the vertical distribution of the modelled current above the continental slope: the vertical current shear is due to the propagation of the different baroclinic modes, mainly the first one, which generates a phase difference across the ray characteristics (see Fig. 9c).

Hence, at the same location, the time evolution of isopycnal interfaces in the top layers and the vertical distribution of the internal tide amplitude and phase are plotted in Figures 17 and 18 respectively. As in the velocity evolution, the model results are nearly in phase with the data: by comparing model and data trough locations in Figure 17, the phase lag is 0.1 day (i.e. 2 h). Between 400 and 1000 m depth the modelled vertical phase variation is in good agreement with the data: the advance in phase of the internal tide in the layers at 1000 m compared with the layers at 400 m is confirmed. The amplitude of the internal tide is of same order of magnitude (50 m) in the data and in the model results. Furthermore, the vertical varia-

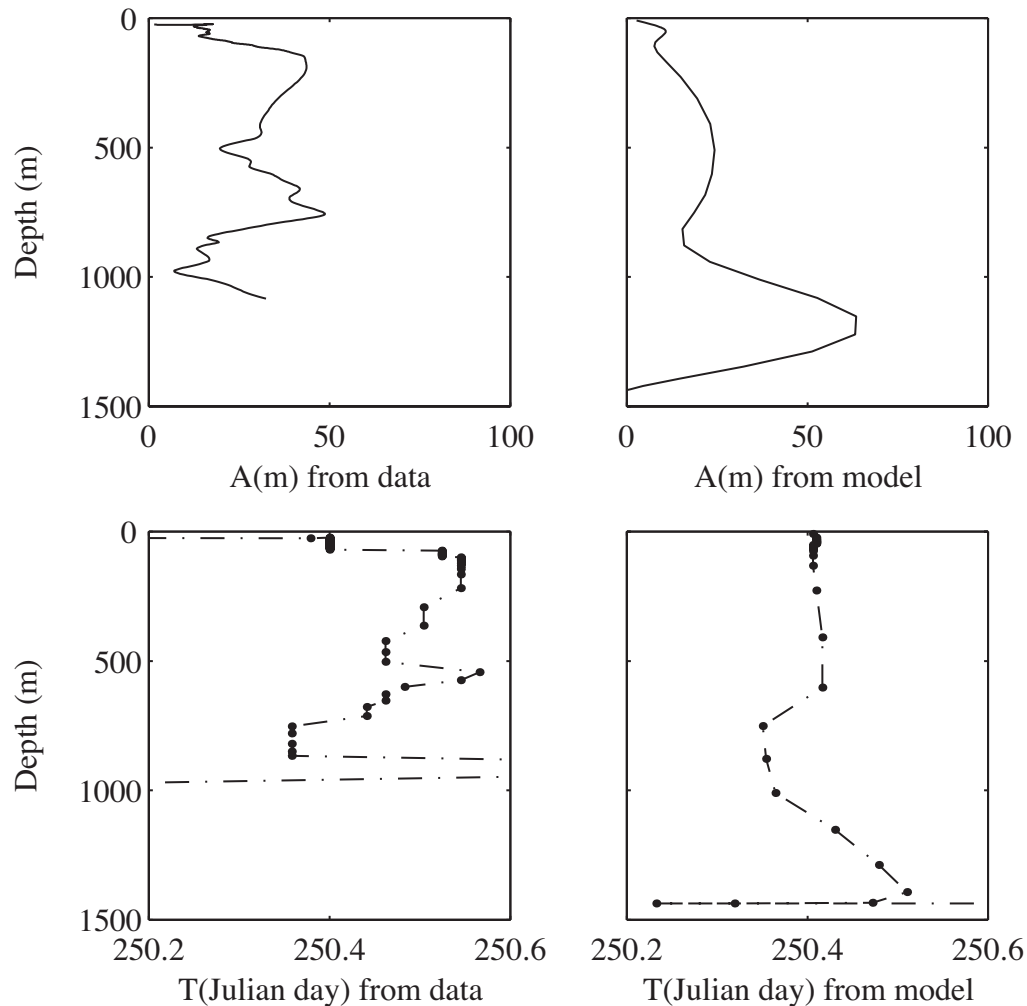


FIG. 18. – Vertical distribution of the estimated amplitude (A) and of the phase (T) of the internal tide from the model and from the observations at the PF06 location. The calculation of A is detailed in *Data/model comparisons* Section. T is the time, in Julian day, when the internal tide trough crosses over PF06.

tion of the modelled internal tide amplitude shows two maxima that are also observed in the data but not at the same depths (maximum values at 500 and 1200 m in the model and at 200 and 800 m in the data). This difference in the vertical distribution is probably due to the spatial resolution of the model: the two points where the comparison is made are not exactly at the same bottom depth (1200 m for the data and 1500 m for the model). In section S2, the variations of the bottom slope near the shelf break are more regular than in section S1 and the resolution of the bathymetry is probably sufficient to well represent the internal tide.

The vertical distribution of the internal tide amplitude and phase is plotted in Figure 19, for PF10. This point is located over the abyssal plain, at the limit of section S2 (Fig. 9), i.e. 180 km off the shelf break. The model results and the data do not

give real information on the vertical distribution of the internal tide amplitude, which is weak compared to PF06, probably due to the damping of the wave. However, even if we are far away from the generation area, the modelled internal tide is nearly in phase with the data in the layers where the comparison is possible (i.e. between 200 and 1300 m).

October stratification case

In October, density data were collected along section S3. The main objective was to point out the differences or similarities between the observed and modelled internal tide phases at locations over the abyssal plain. The phase variations, in term of time evolution and vertical distribution, are compared far away from the generation area in order to estimate the validity of the three-dimensional wave distribution.

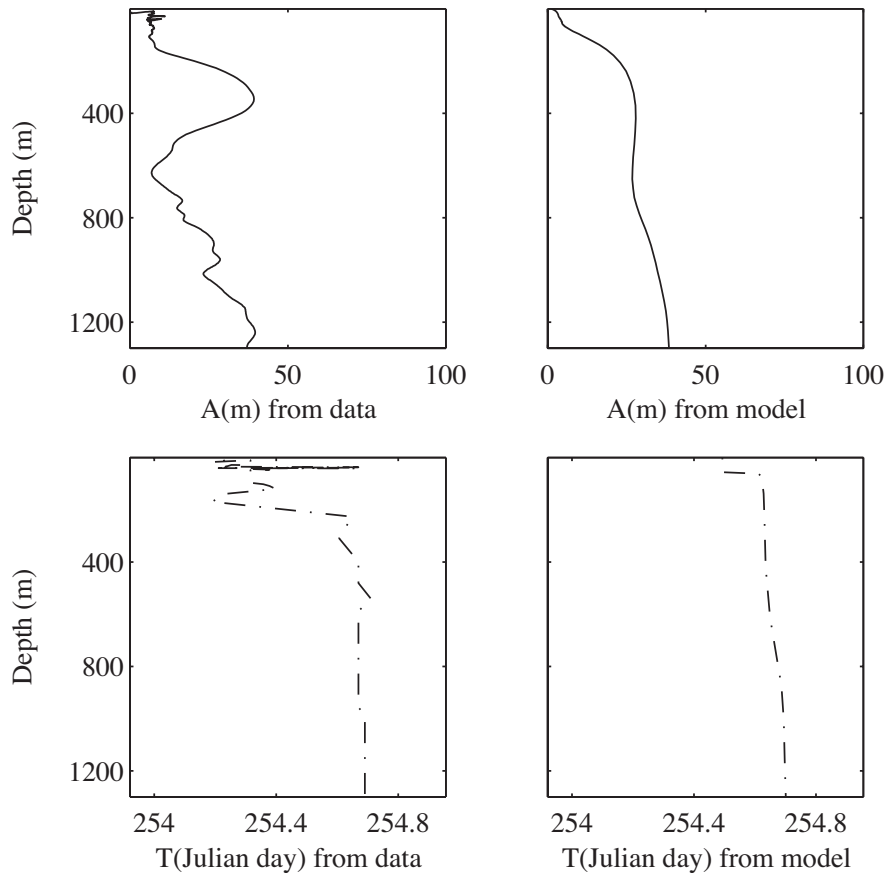


FIG. 19. – Vertical distribution of the estimated amplitude (A) and of the phase (T) of the internal tide from the model and from the observations at the PF10 location. The calculation of A is detailed in *Data/model comparisons* Section. T is the time, in Julian day, when the internal tide trough crosses over PF10.

The time evolution of the isopycnal interfaces inside the seasonal thermocline is displayed in Figure 20, for PF13. The model is less than 2 hours in advance compared with the observations. This difference in the phase of the internal tide is weak and similar to that of the other locations. Moreover, despite the moment of the observation in the tidal cycle (two days after the baroclinic spring tide) and the distance from the generation area (75 km), the modelled internal tide amplitude is still high (40 m from crest to trough) and in agreement with the observations under the thermocline.

In Figure 21, the vertical phase variations show a delay of about 4 hours between the internal tide trough at 1500 m (day 283.2) and the internal tide trough at 200 m (day 283), in the observations as well as in the model results. This numerical result is in agreement with the observations, and also confirms the linear theory of the internal tide propagation (in a flat bottom case), which yields a vertical variation of the internal tide phase across the rays slopes (this one is at 1000 m depth for PF13:

see Fig. 11a). Moreover, as in the linear theory, this vertical phase variation (the delay modelled between the internal tide near the bottom and near the sea surface in agreement with the data) is opposite in sign at PF13 located on an upward ray compared to PF06 located on a downward ray. The vertical distribution of the internal tide amplitude is not really well modelled, particularly in the deep layers, i.e. 1500 and 2500 m, with too high an amplitude compared with the observations. The initial density conditions, which are homogeneous on the horizontal plane, could explain this bias. Indeed, as shown in Figure 11a, PF13 is at the edge of the first upward energetic ray. Therefore, a weak bias in the position of the ray, strongly dependent on the density structure, could explain the differences between the modelled and observed amplitude. This “error” is probably also a consequence of the excessively high barotropic velocity modelled at the top of section S3 (see the data/model comparisons for DP94-2 in *Barotropic tide* Section of *Model results*).

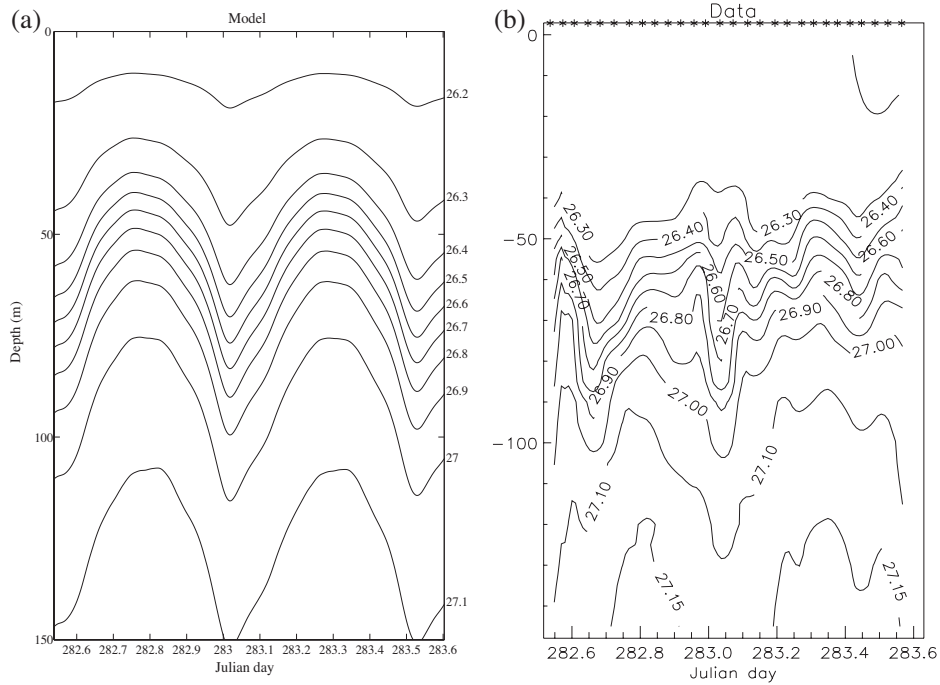


FIG. 20. – Time evolution of isopycnal interfaces from the model (a) and of isopycnal depths from CTD stations between depths of 0 to 150 m (b), during two semi-diurnal tidal cycles at the PF13 location.

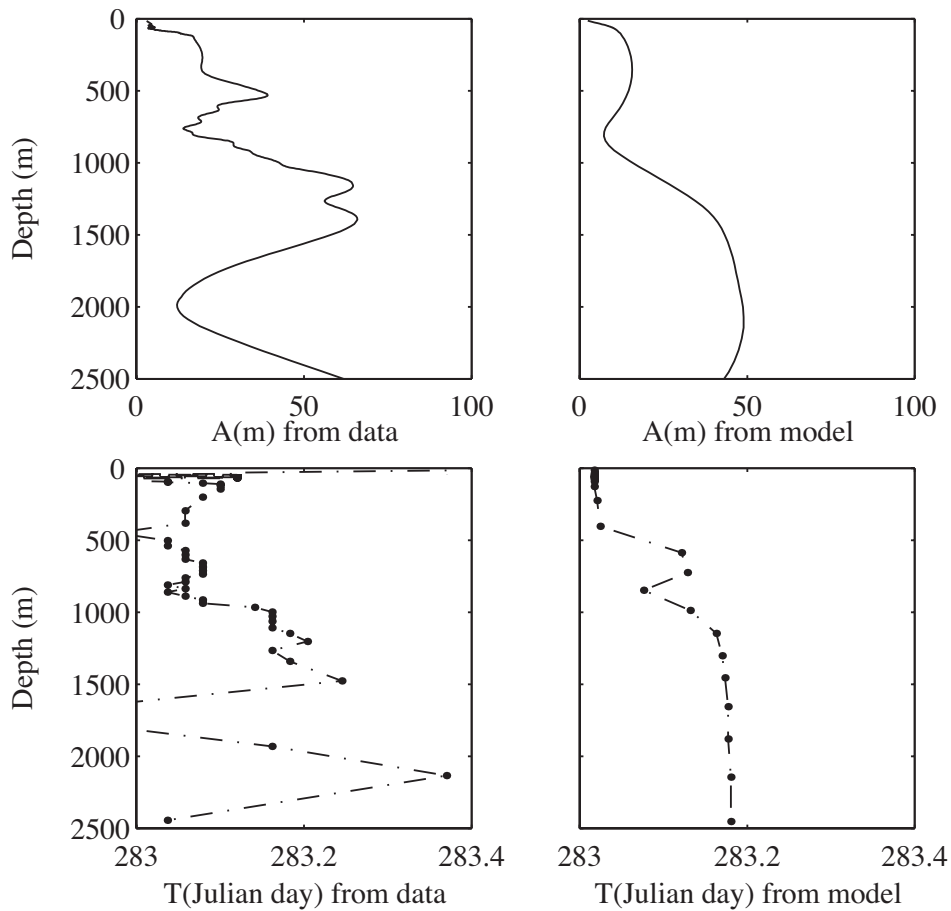


FIG. 21. – Vertical distribution of the estimated amplitude (A) and of the phase (T) of the internal tide from the model and from the observations at the PF13 location. The calculation of A is detailed in *Data/model comparisons* Section. T is the time, in Julian day, when the internal tide trough crosses over PF13.

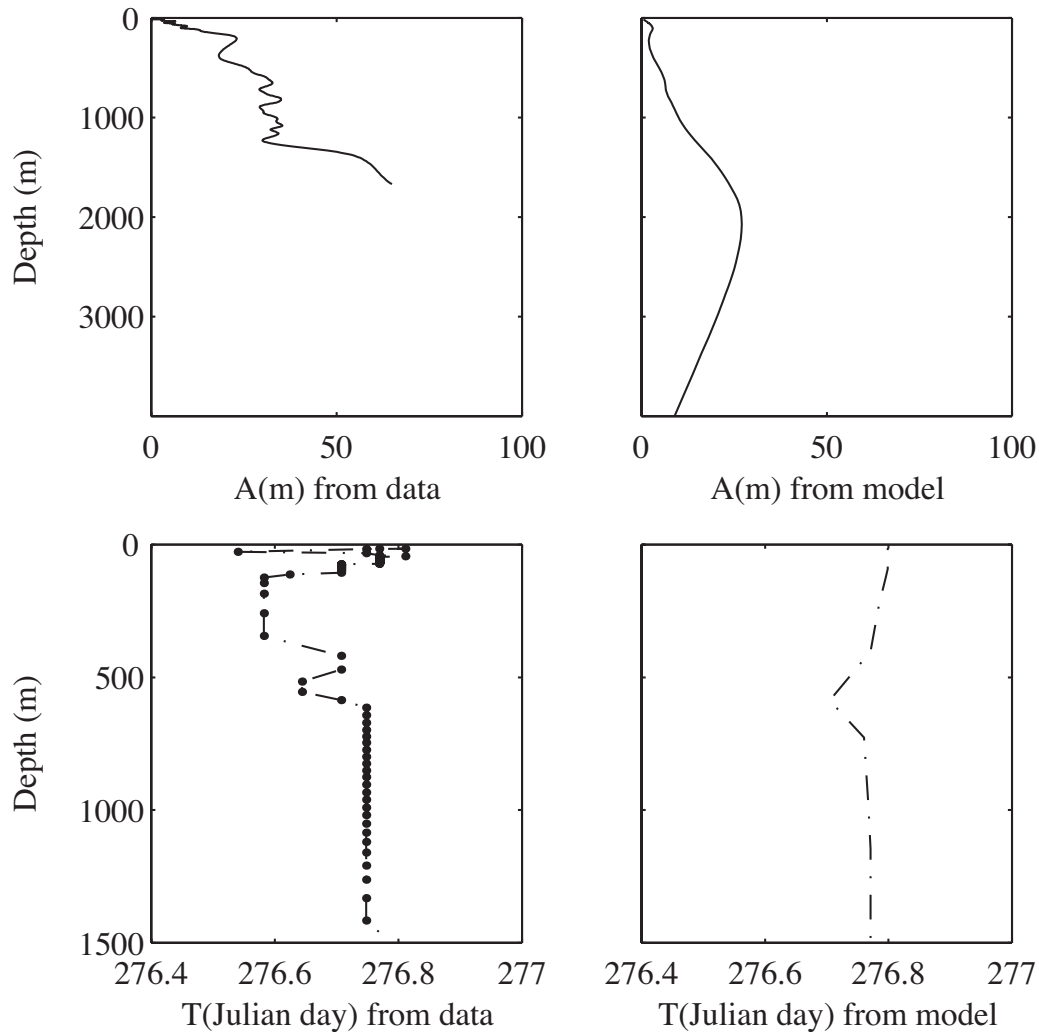


FIG. 22. – Vertical distribution of the estimated amplitude (A) and of the phase (T) of the internal tide from the model and from the observations at the PF14 location. The calculation of A is detailed in *Data/model comparisons* Section. T is the time, in Julian day, when the internal tide trough crosses over PF14.

The data-model comparison at PF14, located 140 km from the French shelf break, is shown in Figure 22, where the vertical variations of internal tide amplitude and phase are plotted. The phase of the internal tide is fairly well modelled, with a trough of the isopycnal levels at almost the same tidal hour (day 276.8: see Fig. 22) as in the data. Moreover, in the observations the vertical variation of the internal tide phase occurs between the depths of 150 and 700 m (Fig. 22), with a delay of the deep layers compared with the upper one. This feature is a result of PF14 location, situated across the second modelled upward ray (see Fig. 11a). Nevertheless, the modelled vertical phase variations do not fit with the data, especially in the upper layers near the sea surface: the assumption of a homogeneous density structure in the horizontal plane probably induces a

bias in the layers which define the seasonal thermocline. The observations were collected four days before the spring tide of the sea surface, i.e. after the neap baroclinic tide if we consider the delay due to the propagation of the wave baroclinic group. This explains the weakness of the internal tide amplitude compared with the PF13 location, in the model as well as in the data. The modelled internal tide amplitude is maximum at 2000 m depth. This increase in the internal tide amplitude at mid-depth, not modelled in the other sections, is probably an effect of the internal tide reflection on the Iberian continental slope (see Fig. 13 and *Baroclinic tide* Section in *Model results*). The data are available only up to 1500 m depth. From 500 to 1500 m, we can only confirm that the observed internal tide amplitude follows the same increase as in the model.

In the October stratification case, the comparisons made far away from the generation area show that the model nearly reproduces the three-dimensional propagation of the internal tide well. However, there is a bias in the predicted internal tide amplitude. The strong across-slope barotropic velocity modelled at the shelf break in section S3, i.e. in the generation area, and the use of an average vertical density profile in the initial conditions are probably the cause of the excessively high predicted amplitude.

DISCUSSION

In this study, the three-dimensional distribution of the internal tides modelled in the Bay of Biscay by MICOM is compared with observations. The whole internal tide process is strongly dependent on the barotropic forcing term, i.e. the tidal velocity in the generation area, mainly situated near the shelf break. Therefore, the barotropic tidal velocity modelled by MICOM in a homogeneous case is compared with measured velocity at the top of the French continental slope. The amplitude of the barotropic current calculated by MICOM at DP94-2 is nearly in agreement with the observations. This is an essential result since DP94-2 is inside the main generation area of internal tides. The resolution of the model is sufficient to have a nearly good forcing term, which is strongly dependent on the local topography. However, the situation of the velocity ellipses is not really in phase with the observations. There is an advance in time of one to two hours between the modelled velocity and the data, which is found again in the modelled internal tide and associated baroclinic current. To have a better fit with the data, we must improve the modelling of the current due to the surface tide, particularly in areas where topographic variations are important and modify the characteristics of the current ellipse.

The modelled results in the stratified cases were more or less similar in September and October, due to the use of an averaged density profile for each period. Therefore, differences in the internal tide distribution which could be induced by the horizontal density variations of the upper layers are not represented.

Over the continental shelf and on the abyssal plain, the internal tides have an effect on the velocity structure. In the Celtic sea, internal tides coming

from areas where the orientation of the bottom continental slope is different produce wave interference: in particular locations, the baroclinic tidal current near the sea surface can reach $\pm 40 \text{ cm s}^{-1}$ in spring tide, which must be added to the barotropic velocity. Therefore, the effect of the internal tide on the continental shelf circulation must be investigated in the future. Over the bottom continental slope, the data/model comparisons at points PF02 and PF06 confirm the influence of the internal tide on the vertical shear of the across-slope velocity. At PF06 in deep layers, this reaches $\pm 15 \text{ cm s}^{-1}$ in the data, a value three times larger than the barotropic tidal current. However, the modelled velocity is weaker than the observations, due to the scheme of the turbulent viscosity intensified by the horizontal shears of current and dependent on the spatial resolution. This numerical weakness acts directly on the velocity amplitude in the whole domain since the highest horizontal current shears due to the internal tides occur in the generation area close to the shelf break. High internal tides are also modelled along a particular section (S3) defined by a line from Ushant to La Coruña. These generate horizontal shears of surface velocity, focused in areas defined by the direction of propagation of the internal tide energy in the vertical plane. Along this section, the modelled amplitude is slightly too high compared with the observations, probably due to an overestimation of the barotropic forcing term on the across-slope component. The importance of realistic modelling is well evidenced along section S1. The model shows evidence of a generation area near the south edge of the Meriadzeck Terrace, where the horizontal tidal current and the internal tide amplitude are intensified near the bottom depth, i.e. by 2400 m of water depth. This feature is confirmed by the observations. The variation of the topography due to the Meriadzeck Terrace also generates different internal tidal waves, which produce interference processes. Hence, the vertical variations of the internal tide phase modelled and observed along sections S2 and S3 are nearly in agreement with the ray theory, with a phase variation that is in opposition at PF06 (downward ray) compared with PF13, PF14 (upward ray).

Nevertheless, the existence and the location of areas in the mid-Bay of Biscay, where the internal tide inside the seasonal thermocline is intensified, must be confirmed by future observations. Furthermore, these areas, which are strongly

dependent on the ray slope, are very sensitive to the stratification introduced as an initial condition. Therefore, the aim of future work is to run the model with an initial three-dimensional density, in order to introduce the spatial variations of the permanent and seasonal pycnoclines between the north and south part of the domain. A realistic density field is also necessary for good modelling of the mixing processes induced by the internal tides.

REFERENCES

- Baines, P.G. – 1982. On internal tide generation models. *Deep-Sea Res.*, 29: 307-338.
- Bleck, R.L. and L. Smith. – 1990. A wind-driven isopycnic coordinate model of the North and Equatorial Atlantic ocean. 1. Model development and supporting experiments. *J. Geophys. Res.*, 95: 3273-3285.
- Craig, P.D. – 1988. A numerical model study of internal tides on the Australian Northwest Shelf. *J. Mar. Res.*, 46: 59-76.
- Cummings, P.F. and L.Y. Oey. – 1997. Simulation of baroclinic and barotropic tides off Northern British Columbia. *J. Phys. Oceanogr.*, 27: 762-781.
- Holloway, P.E. – 1996. A numerical model of internal tides with application to the Australian North West Shelf. *J. Phys. Oceanogr.*, 26: 21-37.
- Holloway, P.E. – 2001. A regional model of the semidiurnal internal tide on to the Australian North West Shelf. *J. Geophys. Res.*, 106: 19,625-19,638.
- Jezequel, N., R. Mazé and A. Pichon. – 2002. Interaction of semi-diurnal tide with a continental slope in a continuously stratified ocean. *Deep-Sea Res.*, 49: 707-734.
- Le Provost C. – 1996. Les marées océaniques le long des côtes européennes. Convention EPSHOM/LEGI n° 7/94.
- Le Tareau, J.Y. and R. Mazé. – 1993. Storm effects on the baroclinic tidal field in the Bay of Biscay. *J. Mar. Sys.*, 4: 327-347.
- Martinsen, E.A. and H. Engedahl. – 1987. Implementation and testing of lateral boundary scheme as an open boundary condition in a barotropic ocean model. *Coastal Eng.*, 11: 603-627.
- Mazé, R. – 1987. Generation and propagation of non-linear internal waves induced by tide over a continental slope. *Cont. Shelf Res.*, 7: 1079-1104.
- New, A.L. – 1988. Internal tidal mixing in the Bay of Biscay. *Deep-Sea Res.*, 35: 691-709.
- New, A.L. and R.D. Pingree. – 1990. Large-amplitude internal soliton packets in the central Bay of Biscay. *Deep-Sea Res.*, 37: 513-524.
- Perenne, N. and A. Pichon. – 1999. Effect of barotropic tidal rectification on low-frequency circulation near the shelf break in the northern Bay of Biscay. *J. Geophys. Res.*, 104: 13,489-13,506.
- Pichon, A. and R. Mazé. – 1992. Passage de la marée au-dessus d'un talus en océan stratifié. *Ann. Hydrogr.*, 18: 65-86.
- Pingree, R.D. and G.T. Mardell. – 1981. Slope turbulence, internal waves and phytoplankton growth at the Celtic Sea shelf-break. *Phil. Trans. R. Soc.*, 302: 663-682.
- Pingree, R.D., G.T. Mardell and A.L. New. – 1986. Propagation of internal tides from the upper slopes of the Bay of Biscay. *Nature*, 321: 154-158.
- Pingree, R.D. and A.L. New. – 1989. Downward propagation of internal tidal energy into the Bay of Biscay. *Deep-Sea Res.*, 36: 735-758.
- Pingree, R.D. and A.L. New. – 1991. Abyssal penetration and bottom reflection of internal tidal energy in the Bay of Biscay. *J. Phys. Oceanogr.*, 21: 28-39.
- Prinsenbergh, S.J. and W.M. Rattray. – 1975. Effects of continental slope and variable Brünt-Väisälä frequency on the coastal generation of internal tides. *Deep-Sea Res.*, 22: 251-263.
- Robertson, R. – 2001. Internal tides and baroclinicity in the southern Weddell sea, 1. Model description. *J. Geophys. Res.*, 106: 27,001-27,016.
- Serpette, A. and R. Mazé. – 1989. Internal tides in the Bay of Biscay : a two-dimensional model. *Cont. Shelf Res.*, 9: 795-821.
- Sherwin, T.J. and N.K. Taylor. – 1990. Numerical investigations of linear internal tide generation in the Rockall Trough. *Deep-Sea Res.*, 37: 1595-1618.
- Smith, L.T. – 1992. Numerical simulations of stratified rotating flow over finite amplitude topography. *J. Phys. Oceanogr.*, 22: 686-696.
- Xing, J. and A.M. Davies. – 1996. Processes influencing the internal tide, its higher harmonics, and tidally induced mixing on the Malin-Hebrides shelf. *Prog. Oceanogr.*, 38: 155-204.
- Xing, J. and A.M. Davies. – 1998a. A three-dimensional model of internal tides on the Malin-Hebrides shelf and shelf edge. *J. Geophys. Res.*, 103, 27: 821-847.
- Xing, J. and A.M. Davies. – 1998b. Influence of stratification upon diurnal tidal currents in the shelf edge regions. *J. Phys. Oceanogr.*, 28: 1803-1831.

Received July 4, 2002. Accepted November 24, 2004.